A Mechanistic Model of the Actin Cycle

M. Bindschadler,* E. A. Osborn,† C. F. Dewey Jr.,† and J. L. McGrath*
*Department of Biomedical Engineering, University of Rochester, Rochester, New York 14642; and †Fluid Mechanics Laboratory, Department of Mechanical Engineering, Massachusetts Institute of Technology, Cambridge, Massachusetts 02139

ABSTRACT We have derived a broad, deterministic model of the steady-state actin cycle that includes its major regulatory mechanisms. Ours is the first model to solve the complete nucleotide profile within filaments, a feature that determines the dynamics and geometry of actin networks at the leading edges of motile cells, and one that has challenged investigators developing models to interpret steady-state experiments. We arrived at the nucleotide profile through analytic and numerical approaches that completely agree. Our model reproduces behaviors seen in numerous experiments with purified proteins, but allows a detailed inspection of the concentrations and fluxes that might exist in these experiments. These inspections provide new insight into the mechanisms that determine the rate of actin filament treadmilling. Specifically, we find that mechanisms for enhancing Pi release from the ADP·Pi intermediate on filaments, for increasing the off rate of ADP-bound subunits at pointed ends, and the multiple, simultaneous functions of profilin, make unique and essential contributions to increased treadmilling. In combination, these mechanisms have a theoretical capacity to increase treadmilling to levels limited only by the amount of available actin. This limitation arises because as the cycle becomes more dynamic, it tends toward the unpolymerized state.

INTRODUCTION

Actin filaments determine cell shape by both supporting and generating mechanical stresses at the cell periphery. Although actin is not modified directly by the signaling pathways that control cell shape, a number of the proteins that bind actin are. These proteins act at the ends or sides of actin filaments to determine the extent and localization of actin polymerization. Although decades of biochemical discovery have provided a literature rich with details on the mechanisms and kinetics of important actin binding proteins, understanding the combined effects of these proteins is difficult without a mathematical framework to organize the information. To this end, we have developed a mathematical model of the steady-state actin cycle that includes the activities of actin and its key mechanisms of regulation. Ours is the first model to predict the full nucleotide composition of steady-state filaments, a feature increasingly recognized as an important determinant of the geometry and dynamics of actin networks (Pollard et al., 2000; Sablin et al., 2002).

The dynamic cycle of actin filament turnover in cells is a complex extension of an ATP-powered cycle intrinsic to purified actin (Stossel, 1993). An actin monomer bound to either ATP or ADP can associate with biochemically distinct ''barbed'' and ''pointed'' ends of an actin filament (Huxley, 1963; Woodrum et al., 1975). After the assembly of ATP-bound monomer, hydrolysis of ATP to ADP·Pi occurs quickly compared to the subsequent release of Pi to form ADP (Carlier and Pantaloni, 1986). Actin polymerization proceeds until only a small concentration ($\sim$0.1 μM) of unpolymerized actin (G-actin) remains. This ''critical concentration'' is also the minimum concentration required to form filaments (F-actin) (Oosawa and Asakura, 1962). Because of ATP hydrolysis within filaments, polymerization proceeds to a steady state rather than a simple equilibrium (Wegner, 1976). At steady state, there is net assembly of ATP-bound actin at barbed ends and net disassembly of ADP-bound subunits at pointed ends. Subunits therefore flux from barbed to pointed ends in a process described as ''treadmilling'' (Kirschner, 1980). After disassembly, ADP-bound actin monomers are recharged with ATP to complete the actin cycle. Although the existence of treadmilling follows from rate constants known for many years (Wegner, 1976; Pollard, 1986), it has been visualized on individual filaments only recently (Fujiwara et al., 2002).

Both regulated and unregulated actin binding proteins modify the actin cycle in cells (Fig. 1). Barbed-end binding proteins block the assembly of G-actin at filament-barbed ends. The most abundant barbed-end binding proteins, capping protein (CP) and gelsolin (Isenberg et al., 1980; Yin et al., 1981), are inactivated by phosphatidylinositol 4,5-bisphosphate (PIP_2) and other polyphosphoinositides (Heiss and Cooper, 1991; Janmey and Stossel, 1987). Gelsolin, which also severs actin filaments (Yin and Stossel, 1979), requires micromolar calcium for its activity. CP, gelsolin, and Arp2/3 complex (Mullins et al., 1998), can nucleate new actin filaments. The processes of severing and nucleation help determine the number and length of actin filaments. Arp2/3 complex can also cap pointed ends (Mullins et al., 1998). Arp2/3 complex activities are greatly enhanced by the GTPase binding protein N-WASp (Machesky et al., 1999; Yarar et al., 1999). Inhibited by phosphorylation (Morgan et al., 1993), the ADF/cofilin family proteins bind preferentially to ADP containing subunits (Carlier et al., 1997). Cofilin destabilizes filaments by severing them (Maciver et al., 1991), by accelerating the rate of ADP subunit disassembly (Carlier

Submitted April 17, 2003, and accepted for publication January 6, 2004.

This article is dedicated to the memory of James F. McGrath.

Address reprint requests to Dr. James L. McGrath, Dept. of Biomedical Engineering, University of Rochester, 601 Elmwood Ave., PO Box 639, Rochester, NY 14642. Tel.: 585-253-5489; Fax: 585-273-4746; E-mail: jmcgrath@bme.rochester.edu.

0006-3495/04/05/2720/20 $2.00

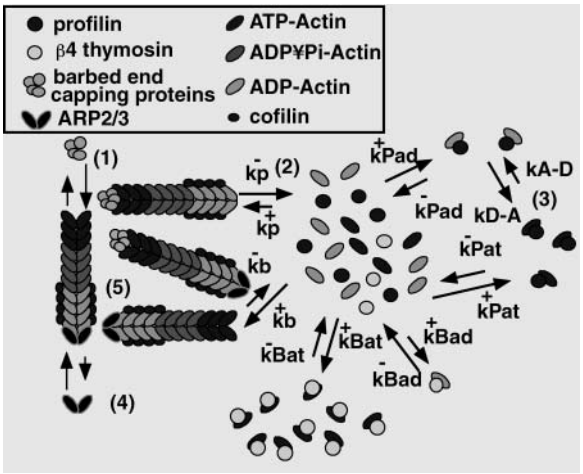

FIGURE 1 Schematic of the actin cycle. Actin-binding proteins regulate actin assembly and disassembly. Regulated proteins control: (*1*) the exposure of barbed ends (capping protein); (*2*) the rate of ADP subunit disassembly and Pi release (cofilin); (*3*) the rate of ADP/ATP nucleotide exchange on G-actin and the amount of G-actin available for polymerization at barbed ends (profilin); (*4*) the exposure of pointed ends (Arp2/3 complex); and (*5*) the number of filaments (gelsolin, Arp2/3 complex, and cofilin). β_4-thymosin acts as a passive sequestering protein preventing G-actin assembly at free pointed ends.

et al., 1997), and by enhancing the rate of Pi release (Blanchoin and Pollard, 1999). Unregulated proteins of the β_4-thymosin family bind actin monomer to maintain unpolymerized actin in some cells at hundreds of times the critical concentration (Safer et al., 1990). Unlike β_4-thymosin, the monomer binding protein profilin has catalytic functions. Profilin accelerates the exchange of ADP for ATP on actin monomer 140-fold (Selden et al., 1999). Unlike actin complexed with β_4-thymosin, profilin-bound G-actin assembles at barbed ends but not pointed ends (Pollard and Cooper, 1984), releasing unbound profilin (Pantaloni and Carlier, 1993). Profilin's activities are inhibited by PIP_2 (Lassing and Lindberg, 1985).

Dufort and Lumsden (1996) first modeled the effects of several actin binding proteins on the steady-state actin cycle. Their model describes the steady-state actin cycle in a homogeneous solution with regulation by profilin and CPs. In contrast, network growth models can describe the growth of lamellipodia or the actin-based motility of *Listeria* as the result of actin assembly modified by several actin-binding proteins (Carlsson, 2001; Mogilner and Edelstein-Keshet, 2002). These system-specific models, however, are not extendable to the full diversity of actin structures and dynamics in cells. To achieve a more general model, we believe the steady-state, homogeneous model of Dufort and Lumsden is the correct starting point. Dufort and Lumsden did not examine several mechanisms that were unknown or underappreciated when their model was developed. Further, Dufort and Lumsden estimate the nucleotide identity of filament termini from the rates of ATP and ADP monomer assembly. We find this assumption seriously overestimates the fraction of barbed ends bound to ADP subunits.

Using established rate constants and other results from the literature, we have constructed a comprehensive model of the actin cycle that reproduces steady-state behaviors seen in numerous experiments with purified actin. Our model allows an intimate look at the nucleotide composition of filaments and the concentration of monomer species as the cycle is modulated at known points of regulation. The inspections also identify the parameters that limit the rate of subunit flux with various mechanisms of regulation. Simulations reveal that ADP subunit disassembly from filament-pointed ends limits the rate of flux in the unregulated cycle to ~0.2 subunit/s and that profilin's activities modestly complement accelerated ADP subunit disassembly to achieve a maximum steady-state flux of ~2.6 subunit/s (4 μM total actin and 0.002 μM filaments). At this maximum, the cycle is limited by Pi release on filaments, illustrating an important connection between two functions of ADF/cofilin. More generally, we find that the mechanisms of enhanced Pi release, accelerated ADP disassembly, and the multiple effects of profilin display a complex synergy in working toward the common goal of enhancing ADP subunit disassembly at pointed ends. In theory, the combination of these mechanisms is limited in its ability to increase flux only by the amount of available actin.

ASSUMPTIONS, IDEALIZATIONS, AND SIMPLIFICATIONS

The literature concerning actin and its regulation is long, rich, and quantitative, but controversies continue and assumptions are required for a broad model. To maximize the clarity and flexibility of the model for revisions, we collect many of our key assumptions here. Other decisions that limit and define our model are introduced as they become relevant to the presentation of the mathematical model (below).

The cycle occurs in a background of excess Mg^{2+}-ATP

We are concerned with matching experiments on purified F-actin that use Mg^{2+} and ATP in concentrations that exceed actin concentrations by at least 20-fold. In these experiments, nucleotide-free actin can be neglected (Kinosian et al., 1993), the rate at which monomers exchange ADP for ATP simplifies to the disassociation rate of Mg^{2+}-ADP on G-actin, and the exchange of ATP for ADP on G-actin can be neglected (Kinosian et al., 1993). These simplifications apply until the sample is aged for several filament turnover times when buildup of free ADP in solution is not negligible.

Inorganic phosphate is released immediately upon disassembly of ADP·Pi subunits

Inorganic phosphate (Pi) binds ADP-G-actin with very low (100 mM) affinity (Wanger and Wegner, 1987). It is likely that this low affinity is at least partly due to a very fast off

rate, and so the assumption of immediate Pi release upon ADP·Pi subunit disassembly is both simplifying and reasonable. The low affinity of Pi for the ADP-G-actin also means ADP·Pi-G-actin is not likely to be generated by the association of Pi with ADP-G-actin in purified solutions (or even in cells where Pi levels are measured at 2–5 mM (Burt et al., 1977)). We will also assume it is not significantly generated by the hydrolysis of ATP on G-actin, although we could only find a literature source showing a very slow rate of hydrolysis on Ca^{2+}-ATP-G-actin (8×10^{-6} s^{-1}; Brenner and Korn, 1980).

Because of a lack of direct evidence for immediate Pi release, it is worth considering an alternative possibility that the ADP·Pi-G-actin species is long-lived and equivalent to ATP-G-actin with respect to its interactions with actin and other proteins (see ''Rate constants'' below for justification of the equivalence assumption). To leave open this possibility, we have included the ADP·Pi-G-actin species in our mathematical model. For our results, we assume immediate release by setting the rate Pi disassociation from ADP·Pi-G-actin to a value orders of magnitude higher than any other rate in the cycle (10,000 s^{-1}).

With the assumption of immediate Pi release, disassociated ADP·Pi subunits produce ADP-G-actin. As the rate of ADP-G-actin produced by this mechanism exceeds the rate of ADP/ATP exchange on G-actin, ADP-G-actin levels elevate, filaments depolymerize, and flux slows (see Fig. 5). These effects are reduced with the assumption of a long-lived ADP·Pi-G-actin species (not shown). They are also reduced by assuming an ADP disassociation rate on monomer 10-fold higher than the most common value from the literature of $k_{mD\rightarrow T} = 0.01$ s^{-1} (Kinosian et al., 1993; Selden et al., 1999; Teubner and Wegner, 1998). There are literature sources reporting ADP disassociation rates on monomer that are eightfold (Blanchoin and Pollard, 1998) and 20-fold (Perelroizen et al., 1996) higher than the common value. Methodological differences likely account for the differences in literature values because the fluorescent analogs used bind actin more weakly than native nucleotides (Neidl and Engel, 1979) and their binding is sensitive to pH and salts (Selden et al., 1999).

The assumption of immediate Pi release is justified here because our model mimics well-documented behaviors of steady-state actin without deviating from consensus rates or introducing a new species. However if future experiments reveal quantitative disparities, these alternative possibilities should be considered.

Hydrolysis of ATP within filaments occurs randomly

There remains debate over whether, in the presence of Mg^{2+}, ATP hydrolysis occurs randomly within filaments or requires an interface between ATP subunits and non-ATP subunits. The latter scenario is termed vectorial hydrolysis because the interface is likely to be a sharp boundary between recently assembled ATP monomer and older and more interior ADP and ADP·Pi subunits. The idea of vectorial hydrolysis was inspired by data indicating a nearly constant rate of hydrolysis regardless of the amount of ATP subunits assembled (Carlier et al., 1987). Such data suggest a limiting value for hydrolysis at a single site within the filament. However, more recent work that intentionally introduced multiple interfaces by copolymerizing ATP and ADP did not find a concurrent increase in the rate of hydrolysis (Pieper and Wegner, 1996), and in general the more recent data, including those obtained with a high resolution quenched-flow device (Blanchoin and Pollard, 2002), do not resemble the data that inspired the vectorial hypothesis. For these reasons, our model defaults to the assumption of random hydrolysis and we use the rate of 0.3 s^{-1} at both the barbed and pointed ends (Blanchoin and Pollard, 2002). However, to compare the hydrolysis mechanisms, we have also modeled the vectorial mechanism using the original rate constants of Carlier et al. (1987).

Rate constants for actin assembly/disassembly

One extensive effort by Pollard (1986) reports the assembly and disassembly rate constants for actin at both barbed and pointed filament ends in the presence of either ATP or ADP (eight constants: k_{bD}^{-}, k_{bD}^{+}, k_{pD}^{-}, k_{pD}^{+}, k_{bT}^{-}, k_{bT}^{+}, k_{pT}^{-}, and k_{pT}^{+}; see Table 1 for definitions). We use these constants but adjust k_{pD}^{-} from 0.27 s^{-1} to 0.3 s^{-1} to match the ADP critical concentrations at the barbed and pointed end ($CC_{bD} = k_{bD}^{-}/k_{bD}^{+} = CC_{pD} = k_{pD}^{-}/k_{pD}^{+}$), as is thermodynamically required by the ADP-equilibrium polymer. The remaining constants are derived from an assumed equivalence between ATP-actin and ADP·Pi-actin $k_{bD\cdot Pi}^{-} = k_{bT}^{-}$, $k_{bD\cdot Pi}^{+} = k_{bT}^{+}$, $k_{pD\cdot Pi}^{-} = k_{pT}^{-}$, and $k_{pD\cdot Pi}^{+} = k_{pT}^{+}$. The equivalence between ATP-actin and ADP·Pi actin is consistent with structural models showing similar conformations for ATP and ADP·Pi-G-actin that are both distinguishable from ADP-G-actin (Otterbein et al., 2001), and the fact that the critical concentration for the ADP·Pi equilibrium polymer equals the ATP barbed-end critical concentration (Rickard and Sheterline, 1986; Wanger and Wegner, 1987).

We note there are ATP and ADP·Pi equilibrium polymers for which the rate constants must satisfy no-energy/no-flux conditions: $CC_{bT} = k_{bT}^{-}/k_{bT}^{+} = CC_{pT} = k_{pT}^{-}/k_{pT}^{+}$ and $CC_{bD\cdot Pi} = k_{bD\cdot Pi}^{-}/k_{bD\cdot Pi}^{+} = CC_{pD\cdot Pi} = k_{pD\cdot Pi}^{-}/k_{pD\cdot Pi}^{+}$. However the rate constants reported by Pollard (1986) and others show severalfold lower ATP critical concentration at the barbed end of filaments compared to the pointed end, and we conclude that at least some of the measured rate constants do not apply to the equilibrium polymers. We are justified in choosing the nonequilibrium rates because treadmilling is a perpetual nonequilibrium state. One challenging possibility is that under certain conditions, our simulations may tend

TABLE 1 Variable and parameter definitions

Variable	Description
at	Concentration of ATP-bound unpolymerized actin
ad	Concentration of ADP-bound unpolymerized actin
$adpi$	Concentration of ADP·Pi-bound unpolymerized actin
f	Concentration of actin in filaments
n	Concentration of filaments
$Atot$	Total concentration of actin
$Btot$	Total concentration of β_4-thymosin
$Ptot$	Total concentration of profilin
B	Concentration of free β_4-thymosin
Bat	Concentration of ATP-bound monomer complexed with β_4-thymosin
Bad	Concentration of ADP-bound monomer complexed with β_4-thymosin
$Badpi$	Concentration of ADP·Pi-bound monomer complexed with β_4-thymosin
P	Concentration of free profilin
Pat	Concentration of free ATP-bound monomer complexed with profilin
Pad	Concentration of free ADP-bound monomer complexed with profilin
$Padpi$	Concentration of free ADP·Pi-bound monomer complexed with profilin
α	Fraction of barbed ends capped
β	Fraction of pointed ends capped
$g_{\mathrm{bT(i)}}$	Fraction of subunits at position i near filament barbed ends that are bound to ATP
$g_{\mathrm{bD\cdot Pi(i)}}$	Fraction of subunits at position i near filament barbed ends that are bound to ADP·Pi
$g_{\mathrm{bD(i)}}$	Fraction of subunits at position i near filament barbed ends that are bound to ADP
$g_{\mathrm{pT(i)}}$	Fraction of subunits at position i near filament pointed ends that are bound to ATP
$g_{\mathrm{pD\cdot Pi(i)}}$	Fraction of subunits at position i near filament pointed ends that are bound to ADP·Pi
$g_{\mathrm{pD(i)}}$	Fraction of subunits at position i near filament pointed ends that are bound to ADP
$\vec{q}$	Rate of subunit flux

toward filaments with composition nearly that of an all ATP or ADP·Pi equilibrium polymer, but because of our use of nonequilibrium rate constants, the system continues to display a higher affinity for G-actin at barbed ends and continues to flux without energy consumption. We can only say that we do not see filaments approaching these equilibrium polymers (all ATP or ADP·Pi) in the simulations reported here, so that our results are at least consistent with our assumptions. Clearly, more measurements are needed to resolve the transition between equilibrium and nonequilibrium rates and arrive at a more complete model. This is one of several areas of future work to which the current model can contribute (see Discussion).

All actin filaments are of the same length

Actin filaments in purified solutions have exponentially distributed lengths (Sept et al., 1999) and so this an unrealistic feature of our model. However, the calculation of nucleotide profiles for a polydisperse solution is a significant challenge that we defer to a future model. The simplification will have no consequences if the dynamics of actin solutions depend on the number of filaments but not on their lengths. Since these dynamics are determined by the interactions between terminal subunits and the monomer pool, the impact of the simplification really depends on whether the terminal identities depend on filament length. In general, the pointed and barbed ends both contribute to the nucleotide profile and the influence of one end on the opposite end is greater as the ends approach each other in shorter filaments. However, long and/or slowly cycling filaments should have an internal ADP core that insulates the ends from each other. Changes in filament lengths that only change the length of this core can have no impact in our model. Thus we suspect that this simplification more adversely impacts our quantitative predictions for short and/or highly dynamic filaments.

Profilin-actin deposits ATP-bound subunits at barbed ends and then instantly decouples from filaments

Although there is a consensus that the profilin-ATP-G-actin complex assembles at barbed ends with rates equivalent to ATP-G-actin, there is debate over whether this addition is linked to ATP hydrolysis. In one view, the addition of profilin-ATP-G-actin catalyzes the hydrolysis of ATP to ADP·Pi on F-actin (Pantaloni and Carlier, 1993). The low affinity of profilin for ADP·Pi-F-actin then explains why profilin so rapidly dissociates from filaments that it fails to act as a cap that hinders subsequent assembly (Gutsche-Perelroizen et al., 1999). Others argue that profilin-actin assembly is a more exact analog of G-actin assembly and is not linked to hydrolysis (Kang et al., 1999). In this case the rapid uncoupling of profilin from ATP subunits after assembly explains why profilin fails to cap. This view is supported by recent data showing that profilin-actin assembly outpaces ATP hydrolysis in rapidly assembling filaments (Blanchoin and Pollard, 2002). We adopt the latter view and assume that profilin instantly decouples from barbed ends to leave an ATP, rather than an ADP·Pi, subunit at the barbed-end terminus.

MATHEMATICAL MODEL

Monomer/filament interactions in the absence of accessory proteins

The mathematical system describing the steady-state interaction between G-actin and filaments in the absence of accessory proteins is:

$$\begin{aligned}\frac{d}{dt}[f] = 0 = {} & k_{\mathrm{bT}}^{+}[at] + k_{\mathrm{bD\cdot Pi}}^{+}[adpi] + k_{\mathrm{bD}}^{+}[ad] - k_{\mathrm{bT}}^{-}g_{\mathrm{bT(1)}} \\ & - k_{\mathrm{bD\cdot Pi}}^{-}g_{\mathrm{bD\cdot Pi(1)}} - k_{\mathrm{bD}}^{-}g_{\mathrm{bD(1)}} + k_{\mathrm{pT}}^{+}[at] + k_{\mathrm{pD\cdot Pi}}^{+}[adpi] \\ & + k_{\mathrm{pD}}^{+}[ad] - k_{\mathrm{pT}}^{-}g_{\mathrm{pT(1)}} - k_{\mathrm{pD\cdot Pi}}^{-}g_{\mathrm{pD\cdot Pi(1)}} - k_{\mathrm{pD}}^{-}g_{\mathrm{pD(1)}} \quad (1)\end{aligned}$$

$$\frac{d}{dt}[ad] = 0 = k_{mD\cdot Pi\rightarrow D}[adpi] - kdt[ad] + [n] \times (k^{-}_{pD}g_{pD(1)} - k^{+}_{pD}[ad] + k^{-}_{bD}g_{bD(1)} - k^{+}_{bD}[ad]) \quad (2)$$

$$\frac{d}{dt}[adpi] = 0 = -k_{mD\cdot Pi\rightarrow D}[adpi] + [n](k^{-}_{pD\cdot Pi}g_{pD\cdot Pi(1)} - k^{+}_{pD\cdot Pi}[adpi] + k^{-}_{bD\cdot Pi}g_{bD\cdot Pi(1)} - k^{+}_{bD\cdot Pi}[adpi] \quad (3)$$

$$Atot = [at] + [ad] + [adpi] + [f] \quad (4)$$

$$1 = g_{pD\cdot Pi(1)} + g_{pD(1)} + g_{pT(1)} \quad (5)$$

$$1 = g_{bD\cdot Pi(1)} + g_{bD(1)} + g_{bT(1)}. \quad (6)$$

All symbols are defined in Tables 1 and 2. We indicate the fractional nucleotide content of subunits within filaments with the notation $g_{eN(i)}$. Here e is assigned a value of b or p for barbed or pointed ends, respectively, N is either T (ATP), D (ADP), or $D{\cdot}Pi$ (ADP·Pi), and the subscript (i) identifies the subunit position within the filament with $i = 1$ signifying the terminal subunit. Finally, g is the fraction of all filaments ($0 \leq g \leq 1$) with nucleotide N at position i counting from end e. Since the G-actin pool only interacts with the filament termini, $i = 1$ in the above system. The first equation demands no net assembly of actin filaments at steady state. The next equations require no net formation of ADP-G-actin and ADP·Pi-G-actin. They account for intrinsic nucleotide exchange on G-actin and an assumed release of Pi from ADP·Pi monomers. The fourth equation conserves total actin, and the final equations state that terminal subunits are bound to one of three possible nucleotides.

ATP hydrolysis and the nucleotide composition of filaments

The nucleotide bound to terminal subunits depends in a complex way on the identity of both assembling G-actin and interior subunits. To describe this dependence, we consider three events that can change the nucleotide species bound to the ith subunit. First, the terminal subunit can disassociate to expose an interior subunit. Our model accounts for this event by renumbering the remaining subunits so that nucleotide fraction at $i + 1$ becomes the nucleotide fraction at subunit i. Similarly, assembly events renumber subunits so that the species bound to subunit $i - 1$ becomes the species at location i. Species conversions also occur as Pi releases randomly from ADP·Pi subunits and as ATP is hydrolyzed to ADP·Pi randomly (in our standard model). Thus at steady state the balanced creation and loss of ATP subunits at barbed-end termini are represented by

$$\frac{d}{dt}g_{bT(1)} = 0 = -k^{-}_{bT}g_{bT(1)}(1 - g_{bT(2)})k^{+}_{bT}[at](1 - g_{bT(1)}) - k^{+}_{bD}[ad]g_{bT(1)} - k^{+}_{bD\cdot Pi}[adpi]g_{bT(1)} + k^{-}_{bD}g_{bD(1)}g_{bT(2)} + k^{-}_{bD\cdot Pi}g_{bD\cdot Pi(1)}g_{bT(2)} - k_{T\rightarrow D\cdot Pi}g_{bT(1)}. \quad (7)$$

In the case of vectorial hydrolysis, the final term is changed to $-k_{bT\rightarrow D\cdot Pi}g_{bT(1)}(1 - g_{bT(2)})$. This form ensures a nucleotide boundary as a prerequisite to hydrolysis. A similar equation ensures no net generation or depletion of ADP-bound termini:

$$\frac{d}{dt}g_{bD(1)} = 0 = k^{+}_{bD}[ad](1 - g_{bD(1)}) - k^{-}_{bD}g_{bD(1)}(1 - g_{bD(2)}) - k^{+}_{bT}[at]g_{bD(1)} - k^{+}_{bD\cdot Pi}[adpi]g_{bD(1)} + k^{-}_{bT}g_{bT(1)}g_{bD(2)} + k^{-}_{bD\cdot Pi}g_{bD\cdot Pi(1)}g_{bD(2)} + k_{fD\cdot Pi\rightarrow D}g_{bD\cdot Pi(1)}. \quad (8)$$

Clearly the solution for terminal subunits requires knowledge of the nucleotide content of the first interior subunit. Similarly, equations written for this interior subunit would reference the second interior subunit. Most generally, for an interior subunit at position i:

$$1 = g_{bD\cdot Pi(i)} + g_{bD(i)} + g_{bT(i)} \quad (9)$$

$$\frac{d}{dt}g_{bT(i)} = 0 = (k^{+}_{bT}[at] + k^{+}_{bD\cdot Pi}[adpi] + k^{+}_{bD}[ad])(g_{bT(i-1)} - g_{bT(i)}) + (k^{-}_{bT}g_{bT(1)} + k^{-}_{bD}g_{bD(1)} + k^{-}_{bD\cdot Pi}g_{bD\cdot Pi(1)}) \times (g_{bT(i+1)} - g_{bT(i)}) - k_{T\rightarrow D\cdot Pi}g_{bT(i)}. \quad (10)$$

$$\frac{d}{dt}g_{bD(i)} = 0 = (k^{+}_{bT}[at] + k^{+}_{bD\cdot Pi}[adpi] + k^{+}_{bD}[ad])(g_{bD(i-1)} - g_{bD(i)}) + (k^{-}_{bT}g_{bT(1)} + k^{-}_{bD}g_{bD(1)} + k^{-}_{bD\cdot Pi}g_{bD\cdot Pi(1)}) \times (g_{bD(i+1)} - g_{bD(i)}) + k_{fD\cdot Pi\rightarrow D}g_{bD\cdot Pi(i)}. \quad (11)$$

In the case of vectorial hydrolysis, the last term in 10 is replaced with: $-k_{bT\rightarrow D\cdot Pi}g_{bT(i)}(1 - g_{bT(i+1)}) - k_{pT\rightarrow D\cdot Pi}g_{bT(i)}(1 - g_{bT(i-1)})$, where we account for both pointed-end and barbed-end facing interfaces.

To completely solve the nucleotide content of filaments, Eqs. 9–11 are written for each subunit and the process is repeated for the pointed end (substituting p for b in Eqs. 7–11). Expansions from the barbed and pointed end eventually meet to share a subunit at $i = i^*$. For continuity between the two filament halves, we require

$$g_{pD(i^*)} = g_{bD(i^*)} \quad (12)$$

$$g_{pD\cdot Pi(i^*)} \quad (13)$$

$$1 = g_{pD\cdot Pi(i^*)} + g_{pD(i^*)} + g_{pT(i^*)} \quad (14)$$

$$1 = g_{bD\cdot Pi(i^*)} + g_{bD(i^*)} + g_{bT(i^*)} \quad (15)$$

and two additional equations that force the values of $g_{bD\cdot Pi(i^*)}$ and $g_{bD(i^*)}$ to reside on a cubic curve passing through the four subunits flanking i^*.

If the total number of subunits in a filament is $\mathcal{L}$, the number of simultaneous equations that must be solved to describe the actin cycle with no regulatory proteins is $3(\mathcal{L}+1)+4$. These equations become M1–M22 in Table 3 with modifications from regulatory proteins.

Analytical solution to the nucleotide composition of filaments

The large system of equations represented by Eqs. 1–15, and M1–M30 in Table 3, are computationally cumbersome. Even for short filaments with $\mathcal{L} = 200$ subunits, 607 simultaneous equations must be solved to determine the internal subunit identities. In seeking simplifications, we note that Eqs. 10 and 11 are difference equations in the nucleotide fractions. In the Appendix, we write difference equations for the ADP·Pi- and ATP-bound fractions and show that the system has the general solution

TABLE 2 Rate constants and literature sources

Constant	Description	Value	References
k_{bT}^{+}	ATP-G-actin association at barbed ends	11.6 $(\mu M\ s)^{-1}$	Pollard (1986)
$k_{bD\cdot Pi}^{+}$	ADP·Pi-G-actin association at barbed ends	11.6 $(\mu M\ s)^{-1}$	Equivalence to ATP-actin (see ''Assumptions'')
k_{bD}^{+}	ADP-G-actin association at barbed ends	3.8 $(\mu M\ s)^{-1}$	Pollard (1986)
k_{pT}^{+}	ATP-G-actin association at pointed ends	1.3 $(\mu M\ s)^{-1}$	Pollard (1986)
$k_{pD\cdot Pi}^{+}$	ADP·Pi-G-actin association at pointed ends	1.3 $(\mu M\ s)^{-1}$	Equivalence to ATP-actin
k_{pD}^{+}	ADP-G-actin association at pointed ends	0.16 $(\mu M\ s)^{-1}$	Pollard (1986)
k_{bT}^{-}	ATP-G-actin disassociation at barbed ends	1.4 s^{-1}	Pollard (1986)
$k_{bD\cdot Pi}^{-}$	ADP·Pi subunit disassociation at barbed ends	1.4 s^{-1}	Equivalence to ATP-actin
k_{bD}^{-}	ADP subunit disassociation at barbed ends	7.2 s^{-1}	Pollard (1986)
k_{pT}^{-}	ATP subunit disassociation at pointed ends	0.8 s^{-1}	Pollard (1986)
$k_{pD\cdot Pi}^{-}$	ADP·Pi subunit disassociation at pointed ends	0.8 s^{-1}	Equivalence to ATP-actin
k_{pD}^{-}	ADP subunit disassociation at pointed ends	0.3 s^{-1}	Calculated from Pollard (1986) (see text)
k_{PD}^{-}	Profilin-ADP-G-actin complex dissociation rate	0.65 s^{-1}	Based on equilibrium constant from Selden et al. (1999)
k_{PD}^{+}	Profilin-ADP-G-actin complex association rate	1 $(\mu M\ s)^{-1}$	Assigned
k_{PT}^{-}	Profilin-ATP-G-actin complex dissociation rate	0.6 s^{-1}	Based on equilibrium constant from Selden et al. (1999)
$k_{PD\cdot Pi}^{-}$	Profilin-ADP·Pi-G-actin complex dissociation rate	0.6 s^{-1}	Equivalence to ATP-actin
k_{PT}^{+}	Profilin-ATP-G-actin association rate	1 $(\mu M\ s)^{-1}$	Assigned
$k_{PD\cdot Pi}^{+}$	Profilin-ADP·Pi-G-actin association rate	1 $(\mu M\ s)^{-1}$	Equivalence to ATP-actin
$k_{mD\rightarrow T}$	Rate of ADP exchange for ATP on free monomer	0.01 s^{-1}	Selden et al. (1999)
$k_{PD\rightarrow T}$	Rate of ADP exchange for ATP on profilin-actin	1.40 s^{-1}	Selden et al. (1999)
$k_{PD\cdot Pi\rightarrow T}$	Rate of ADP·Pi exchange for ATP on profilin-actin	0.08 s^{-1}	Equivalence to ATP-actin
$k_{T\rightarrow D\cdot Pi}$	Rate of ATP hydrolysis on filaments	0.3 s^{-1}	Blanchoin and Pollard (2002)
$k_{fD\cdot Pi\rightarrow D}$	Rate of Pi release from ADP·Pi subunits	0.0026 s^{-1}	Melki et al. (1996)
$k_{mD\cdot Pi\rightarrow D}$	Rate of Pi release from ADP·Pi-G-actin	10,000 s^{-1}	Immediate release of Pi on G-actin
K_{BD}	Equilibrium disassociation constant for β_4-thymosin and ADP-G-actin	100 μM	$k_{BD}^{+} = 1(\mu M\ s)^{-1}$ and $k_{BD}^{-} = 100\ s^{-1}$ assigned; K_{BD} from Carlier et al. (1993)
K_{BT}	Equilibrium disassociation constant for β_4-thymosin and ATP-G-actin	0.9 μM	$k_{BT}^{+} = 1(\mu M\ s)^{-1}$ and $k_{BT}^{-} = 0.9\ s^{-1}$ assigned; K_{BT} from Kang et al. (1999)
$K_{BD\cdot Pi}$	Equilibrium disassociation constant for β_4-thymosin and ADP·Pi-G-actin	0.9 μM	Equivalence to ATP-actin

$$g_{eD\cdot Pi(i)} = A_e(\delta_e^{+})^i + B_e(\delta_e^{-})^i + E_e(\lambda_e^{+})^i + F_e(\lambda_e^{-})^i$$

$$g_{eT(i)} = C_e(\lambda_e^{+})^i + D_e(\lambda_e^{-})^i$$

$$1 = g_{eD\cdot Pi(i)} + g_{eT(i)} + g_{eD(i)},$$

where $\delta_e^{\pm}$ and $\lambda_e^{\pm}$ are the roots of the quadratic characteristic equations derived from the difference equations for the ADP·Pi or ATP nucleotide fractions, respectively. The coefficients E_e and F_e are determined from particular solutions of the nonhomogenous difference equation in ADP·Pi. Finally the eight constants A_e, B_e, C_e, and D_e are found from the boundaries between filaments and the monomer pool at the filament termini and the boundary between pointed- and barbed-end solutions at the center of the filament. Since $\delta_e^{\pm}$ and $\lambda_e^{\pm}$ are constants representing the ratio of adjacent nucleotide fractions, these solutions amount to the sums of discrete exponentials. We find they agree completely with the numerical solution formulated in Eqs. 5–15 but, in the case of a 200-subunit filament without accessory proteins, reduce the number of simultaneously solved equations from 607 to 16. It is important to note that when the analytical solutions to the nucleotide profiles are used, the complete solution is a hybrid between this analytical solution and the numerical solution for the monomer pool and that the two pieces are interdependent and solved simultaneously.

We have not obtained an analytical solution to the ATP profile for the case of vectorial hydrolysis (in this case the resulting difference equation is nonlinear) and this precludes a solution to the nonhomogeneous ADP·Pi difference equation. Therefore to simplify the system for the case of vectorial hydrolysis, we solve the ATP profile numerically for 10 subunits in from either filament end. For more interior subunits, we assume no ATP and solve the homogenous ADP·Pi equation analytically (see Appendix). Using the complete numerical solution, we find that the assumption of an ATP-free core beyond 10 subunits interior to the filament is very conservative for the vectorial hydrolysis numbers reported by Carlier et al. (1987).

Filament concentration as a regulated parameter

The concentration of filaments is increased through the processes of severing, nucleation, and fragmentation and decreased through complete filament depolymerization and annealing. Our model does not explicitly account for these processes, but varies a filament concentration $[n]$ that represents their steady-state balance.

Barbed- and pointed-end capping as regulated parameters

The fraction of barbed or pointed ends available for interactions with monomers are controlled in cells by capping proteins and Arp2/3 complex. Again our representation of these proteins is not explicit. We also do not consider a relationship between pointed-end capping and nucleation even though these are intimately connected functions of active Arp2/3 complex (Mullins et al., 1998). We represent the activities of barbed- and pointed-end

capping by the parameters α and β, respectively. These appear as coefficients multiplying all assembly and disassembly terms at their respective filament ends. Thus α and β are interpreted as the fraction of ends exposed and their values vary between 0 and 1.

Accelerated ADP subunit disassembly as a regulated mechanism

The acceleration of ADP subunit disassembly by the ADF/cofilin family of proteins provides a critical explanation of how cells can accelerate disassembly beyond the rates intrinsic to unregulated actin. To examine the role of accelerated ADP subunit disassembly in our model, we directly increase the pointed-end disassembly rate constant k_{pD}^-. To account for the possibility of an ADP equilibrium polymer and ensure the no-energy/no-flux condition $CC_{bD} = CC_{pD}$, we adjust k_{bD}^- proportionately as k_{pD}^- varies.

Enhanced Pi release as a regulated mechanism

In addition to severing filaments and increasing ADP subunit disassembly, the ADF/cofilin family has been found to increase the rate of Pi release (Blanchoin and Pollard, 1999). We examine this mechanism by varying the rate of Pi release on filaments, $k_{fD\cdot Pi\rightarrow D}$, from its default level of 0.0026 s^{-1} (Melki et al., 1996). We do not consider ADF/cofilin molecules explicitly, and by separating enhanced Pi release, severing, and enhanced ADP subunit disassembly, we artificially distinguish between what are actually simultaneous functions of ADF/cofilin proteins (Blanchoin and Pollard, 1999).

Because we don't represent ADF/coflins explicitly, we also do not account for their high affinity binding to ADP-G-actin monomer (Blanchoin and Pollard, 1998; Didry et al., 1998). This simplification has little consequence for the dynamics since: 1), ADF-ADP-G-actins assemble at both ends of actin filaments at the same rates as ADP-G-actin (Blanchoin and Pollard, 1999) and 2), once assembled these become the ADF-ADP-F-actin species that we implicitly model with elevated disassembly rates. On the other hand, Blanchoin and Pollard (1998) report that ADF/cofilin slows the exchange of ADP for ATP on G-actin by ~10-fold. One difficultly in pursuing this feature is that our value for ADP/ATP exchange on G-actin is ~10-fold lower than the one reported by Blanchoin and Pollard (1998). To incorporate this result would require that we adopt both constants from Blanchoin and Pollard (1998).

Nucleotide exchange and enhanced assembly by profilin

Profilin binds monomeric actin and accelerates the rate of ADP for ATP exchange 140-fold (Selden et al., 1999). With the assumption of high ATP levels, we ignore the exchange of ADP for ATP on profilin-actin by arguments similar to those for unbound actin. Profilin bound to ATP-charged monomer readily assembles at barbed but not pointed ends (Pollard and Cooper, 1984). To analyze the impact of profilin's multiple and connected activities, we model it explicitly. The representation is accomplished with four new equations (M23–M26, Table 3) and the modification of assembly terms throughout the model.

Monomer sequestration by β_4-thymosin

We are interested in exploring the impact of β_4-thymosin sequestration on the actin cycle. To accomplish this, we explicitly represent β_4-thymosin using affinities for ATP/ADP·Pi-G-actin and ADP-G-actin reported by Kang et al. (1999) and Carlier et al. (1993), respectively. We ignore its weak tendency to assemble into filaments (Ballweber et al., 2002; Carlier et al., 1996) or into ternary complexes with profilin and G-actin (Yarmola et al., 2001). Equations M27–M30 in Table 3 model sequestration of ATP-G-actin, ADP·Pi-G-actin, and ADP-G-actin by β_4-thymosin by assuming rapid equilibrium.

Subunit flux

Subunit flux is calculated by determining the net assembly at either barbed or pointed ends. At barbed ends, we write

$$\vec{q} = k_{bT}^+([at] + [Pat]) + k_{bD\cdot Pi}^+([adpi] + [Padpi]) + k_{bD}^+([ad] + [Pad]) - k_{bT}^- g_{bT(1)} - k_{bD\cdot Pi}^- g_{bD\cdot Pi(1)} - k_{bD}^- g_{bD(1)}.$$

Simulation tools and protein levels

The equations in Table 3 were solved using MATLAB (Release 13, The MathWorks, Natick, MA) on a Macintosh 500 MHz G4 Cube. Gradients for all equations were provided to the Levenberg-Marquardt optimization routines provided in MATLAB's Optimization Toolbox. The levels of total actin (4 μM) and the baseline concentration of filaments (2 nM) were chosen to establish conditions similar to the in vitro studies to which we compare our model. The range on the regulated parameters is chosen to reveal the dynamic range of the system around this baseline.

Uniqueness of the solution

We believe there is only one reasonable solution to the system for the following reasons: First, we have only found only a single solution space in which all concentrations are positive despite varying initial guesses by orders of magnitude. Second, for the case of the nucleotide composition of filaments, we have found an analytical solution we know to be unique and this matches our numerical approach completely. Further, when either of these very different methods for filament calculations is used in the complete solution, we get the same results for the monomer populations.

RESULTS

The complete solution to the nucleotide profile is an important advance

The state of nucleotides at the terminal ends of filaments is important for determining the nucleotide content of the monomer population. The challenge of estimating the identity of the termini arises frequently in modeling of actin dynamics, and often a questionable simplification is made. In their steady-state model of the actin cycle, Dufort and Lumsden (1996) assumed that the fraction of terminal barbed ends carrying ADP is equal to the ratio of rate of ADP-G-actin assembly to the total rate of assembly for all species. A similar assumption has been used to interpret steady-state experiments (Selden et al., 1999), and numerous other simplifications can be found in the literature (e.g., Fujiwara et al., 2002; Pantaloni et al., 1984).

To demonstrate the importance of our effort to obtain the complete filament profile, we compare our results for the fraction of barbed ends bound to ADP to the predictions we would obtain using the Dufort and Lumsden assumption in Fig. 2. Clearly there is general disagreement between these approaches over a wide range of parameter values. The disagreement is most conspicuous when the rate of ADP

TABLE 3 Model equations

Equation	Description
M1	No net assembly of filaments
$0 = \alpha[n]\big(k_{bT}^{+}([Pat]+[at]) - k_{bT}^{-}g_{bT(1)} + k_{bD\cdot Pi}^{+}([adpi]+[Padpi]) - k_{bD\cdot Pi}^{-}g_{bD\cdot Pi(1)} + k_{bD}^{+}([ad]+[Pad]) - k_{bD}^{-}g_{bD(1)}\big) + \beta[n]\Big(k_{pT}^{+}[at] - k_{pT}^{-}g_{pT(1)} + k_{pD\cdot Pi}^{+}[adpi] - k_{pD\cdot Pi}^{-}g_{pD\cdot Pi(1)} + k_{pD}^{+}[ad] - k_{pD}^{-}g_{pD(1)}\Big)$	
M2	No net formation of ADP-G-actin
$0 = \beta[n](k_{pD}^{-}g_{pD(1)} - k_{pD}^{+}[ad]) + \alpha[n](k_{bD}^{-}g_{bD(1)} - k_{bD}^{+}([ad]+[Pad])) + k_{PD}^{-}[Pad] - k_{PD}^{+}[P][ad] + k_{BD}^{-}[Bad] - k_{BD}^{+}[B][ad] + k_{mD\cdot Pi\to D}[adpi]$	
M3	No net formation of ADP·Pi-G-actin
$0 = \beta[n](k_{pD\cdot Pi}^{-}g_{pD\cdot Pi(1)} - k_{pD\cdot Pi}^{+}[adpi]) + \alpha[n]\big(k_{bD\cdot Pi}^{-}g_{bD\cdot Pi(1)} - k_{bD\cdot Pi}^{+}([adpi]+[Padpi])\big) + k_{PD\cdot Pi}^{-}[Padpi] - k_{PD\cdot Pi}^{+}[P][adpi] + k_{BD\cdot Pi}^{-}[Badpi] - k_{BD\cdot Pi}^{+}[B][adpi] - k_{mD\cdot Pi\to D}[adpi]$	
M4	Conservation of actin
$Atot = [at]+[ad]+[adpi]+[f]+[Pat]+[Pad]+[Padpi]+[Bat]+[Bad]+[Badpi]$	
M5 (barbed: $e=b$; $\gamma=\alpha$; $\zeta=1$) M6 (pointed: $e=p$; $\gamma=\beta$; $\zeta=0$)	No net formation of ATP-bound termini
$0 = \gamma\big(k_{eT}^{+}([at]+\zeta[Pat])(1-g_{eT(1)}) - k_{eT}^{-}g_{eT(1)}(1-g_{eT(2)}) + (k_{eD}^{-}g_{eD(1)} + k_{eD\cdot Pi}^{-}g_{eD\cdot Pi(1)})g_{eT(2)} - (k_{eD}^{+}([ad]+\zeta[Pad]) + k_{eD\cdot Pi}^{+}([adpi]+\zeta[Padpi]))g_{eT(1)}\big) - k_{T\to D\cdot Pi}g_{eT(1)}$	
M7 (barbed: $e=b$; $\gamma=\alpha$; $\zeta=1$) M8 (pointed: $e=p$; $\gamma=\beta$; $\zeta=0$)	No net formation of ADP-bound termini
$0 = \gamma\big(k_{eD}^{+}([ad]+\zeta[Pad])(1-g_{eD(1)}) - k_{eD}^{-}g_{eD(1)}(1-g_{eD(2)}) - (k_{eT}^{+}([at] + \zeta[Pat]) + k_{eD\cdot Pi}^{+}g_{eD(1)}([adpi]+\zeta[Padpi]))g_{eD(1)} + (k_{eT}^{-}g_{eT(1)} + k_{eD\cdot Pi}^{-}g_{eD\cdot Pi(1)})g_{eD(2)}\big) + k_{fD\cdot Pi\to D}g_{eD\cdot Pi(1)}$	
M9 (barbed: $e=b$; $\gamma=\alpha$; $\zeta=1$) M10 (pointed: $e=p$; $\gamma=\beta$; $\zeta=0$)	Terminal subunits are bound to 1 of 3 nucleotides
$1 = g_{eD\cdot Pi(1)} + g_{eD(1)} + g_{eT(1)}$	
M11 (barbed: $e=b$; $\gamma=\alpha$; $\zeta=1$) M12 (pointed: $e=p$; $\gamma=\beta$; $\zeta=0$)	No net production of ATP at ith subunit ($1 < i < i^*$)
$0 = \gamma\big((k_{eT}^{-}g_{eT(1)} + k_{eD\cdot Pi}^{-}g_{eD\cdot Pi(1)} + k_{eD}^{-}g_{eD(1)})(g_{eT(i+1)} - g_{eT(i)}) + (k_{eT}^{+}([at]+\zeta[Pat]) + k_{eD\cdot Pi}^{+}([adpi]+\zeta[Padpi]) + k_{eD}^{+}([ad]+\zeta[Pad]))(g_{eT(i-1)} - g_{eT(i)})\big) - k_{T\to D\cdot Pi}g_{eT(i)}$	
M13 (barbed: $e=b$; $\gamma=\alpha$; $\zeta=1$) M14 (pointed: $e=p$; $\gamma=\beta$; $\zeta=0$)	No net production of ADP at ith subunit ($1 < i < i^*$)
$0 = \gamma\big((k_{eT}^{-}g_{eT(1)} + k_{eD\cdot Pi}^{-}g_{eD\cdot Pi(1)} + k_{eD}^{-}g_{eD(1)})(g_{eD(i+1)} - g_{eD(i)}) + (k_{eT}^{+}([at]+\zeta[Pat]) + k_{eD\cdot Pi}^{+}([adpi]+\zeta[Padpi]) + k_{eD}^{+}([ad]+\zeta[Pad]))(g_{eD(i-1)} - g_{eD(i)})\big) + k_{fD\cdot Pi\to D}g_{eD\cdot Pi(i)}$	
M15 (barbed: $e=p$) M16 (pointed: $e=p$)	ith subunits are bound to 1 of 3 nucleotides
$1 = g_{eT(i)} + g_{eD\cdot Pi(i)} + g_{eD(i)}$	

(*continued*)

TABLE 3 (*Continued*)

Equation	Description
M17 M18 $g_{\mathrm{bD}(i^*)} = g_{\mathrm{pD}(i^*)} \qquad g_{\mathrm{bD\cdot Pi}(i^*)} = g_{\mathrm{pD\cdot Pi}(i^*)}$	Continuity at i^*
M19 (barbed: $e = p$) M20 (pointed: $e = p$) $1 = g_{\mathrm{eT}(i^*)} + g_{\mathrm{eD\cdot Pi}(i^*)} + g_{\mathrm{eD}(i^*)}$	i^*th subunit is bound to 1 of 3 nucleotides
M21 M22 $g_{\mathrm{eD}(i^*)}$ and $g_{\mathrm{eD\cdot Pi}(i^*)}$ lie on a cubic flanking i^*	Continuity at i^*
M23 $0 = k_{\mathrm{PT}}^{+}[at][P] - k_{\mathrm{PT}}^{-}[Pat] + k_{\mathrm{PD}\to\mathrm{T}}[Pad] - \alpha k_{\mathrm{bT}}^{+}[Pat][n] + k_{\mathrm{PD\cdot Pi}\to\mathrm{T}}[Padpi]$	No net formation of profilin/ATP-actin
M24 $0 = k_{\mathrm{PD\cdot Pi}}^{+}[adpi][P] - k_{\mathrm{PD\cdot Pi}}^{-}[Padpi] - \alpha k_{\mathrm{bD\cdot Pi}}^{+}[Padpi][n] - k_{\mathrm{PD\cdot Pi}\to\mathrm{T}}[Padpi]$	No net formation of profilin/ADP·Pi-actin
M25 $0 = \alpha[\mathrm{n}](k_{\mathrm{BT}}^{+}[Pat] + k_{\mathrm{BD\cdot Pi}}^{+}[Padpi] + k_{\mathrm{BD}}^{+}[Pad]) - k_{\mathrm{pT}}^{+}[\mathrm{at}][P] - k_{\mathrm{PD\cdot Pi}}^{+}[adpi][P]$ $-k_{\mathrm{PD}}^{+}[ad][P] + k_{\mathrm{PT}}^{-}[Pat] + k_{\mathrm{PD\cdot Pi}}^{-}[Padpi] + k_{\mathrm{PD}}^{-}[Pad]$	No net formation of free profilin
M26 $Ptot = [P] + [Pat] + [Pad] + [Padpi]$	Conservation of profilin
M27 $K_{\mathrm{BT}} = ([at][B])/[Bat]$	β_4-thymosin ATP-G-actin equilibrium
M28 $K_{\mathrm{BD}} = ([ad][B])/[Bad]$	β_4-thymosin ADP-G-actin equilibrium
M29 $K_{\mathrm{BD\cdot Pi}} = ([adpi][B])/[Badpi]$	β_4-thymosin ADP·Pi-G-actin equilibrium
M30 $Btot = [B] + [Bat] + [Badpi] + [Bad]$	Conservation of β_4-thymosin

subunit disassembly is elevated, because despite a lower affinity of ADP-G-actin for filaments, the only determinant of ADP-termini in the simplification of Dufort and Lumsden is the ADP-G-actin assembly rate. The assumption works best with profilin because the monomer pool is almost fully charged with ATP. Simplifying assumptions are even more difficult at the pointed end where subunit identities are determined not only by local assembly and disassembly events, but also by subunits that transit the filament after assembling at the barbed end.

The numerical and analytic solutions to the nucleotide profile agree

In Fig. 3 we illustrate complete agreement between the numerical (M5–M30, Table 3) and analytic (Appendix)

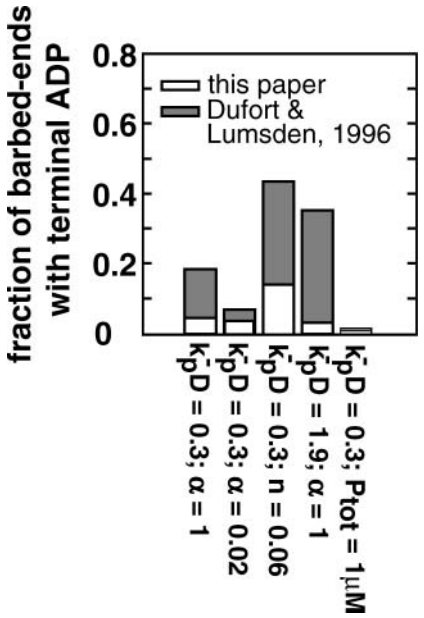

FIGURE 2 Evaluation of the simplification of Dufort and Lumsden (1996). Dufort and Lumsden assumed that the fraction of ADP-termini was in proportion to the ratio of ADP-G-actin assembly to total assembly. This assumption overestimates the fraction of barbed-end ADP-termini in all cases. The disagreement is least pronounced in the presence of profilin, when the ADP monomer pool is small. Unless specified, parameters are set at $\alpha = 1$, $Ptot = 0$ μM, $n = 0.002$ μM, and $Atot = 4$ μM.

solutions to the nucleotide profile of filaments at steady state for filaments 370 subunits (1 μm) in length. We make the comparison with active profilin and elevated ADP subunit disassembly because these conditions produce dynamic profiles. The figure also shows full agreement between the numerical and analytic versions of the vectorial hydrolysis model.

In addition to providing an important check on our work, the figure reveals interesting features in nucleotide profiles. Notable is the polarity of the nucleotide profiles. ATP is only present near the barbed ends and ADP·Pi decays near the barbed end to an ADP-rich interior. Intriguing also is the drop in ADP (and concurrent rise in ADP·Pi) very near the pointed ends. This feature suggests events at the pointed ends have a limited influence on the nucleotide profile under these conditions.

Finally, we note the profiles for random and vectorial hydrolysis are similar but distinctive. In the case of random hydrolysis, ATP persists further into the filament and the ADP·Pi profile displays a prominent peak. It is worth noting that the profiles provide a signature of the hydrolysis mechanism because distinguishing between random and vectorial hydrolysis has been difficult using kinetic data (Blanchoin and Pollard, 2002). Consistent with these difficulties, we find that the two hydrolysis mechanisms give similar fluxes even at very different level of regulation (Table 4).

Varying barbed-end exposure results in experimentally observed behaviors

If our model is a reasonable representation of the steady-state actin cycle, then it must exhibit key behaviors seen in experiments. One important steady-state result is that in actin solutions where barbed ends are all capped, the monomer concentration is roughly the critical concentration of ATP actin at the pointed ends of filaments ($\sim$0.6 μM) (Schafer et al., 1996; Walsh et al., 1984). In these same experiments, decreasing the fraction of barbed ends capped causes net polymerization and reduces the monomer concentrations toward the critical concentration of ATP actin at the barbed

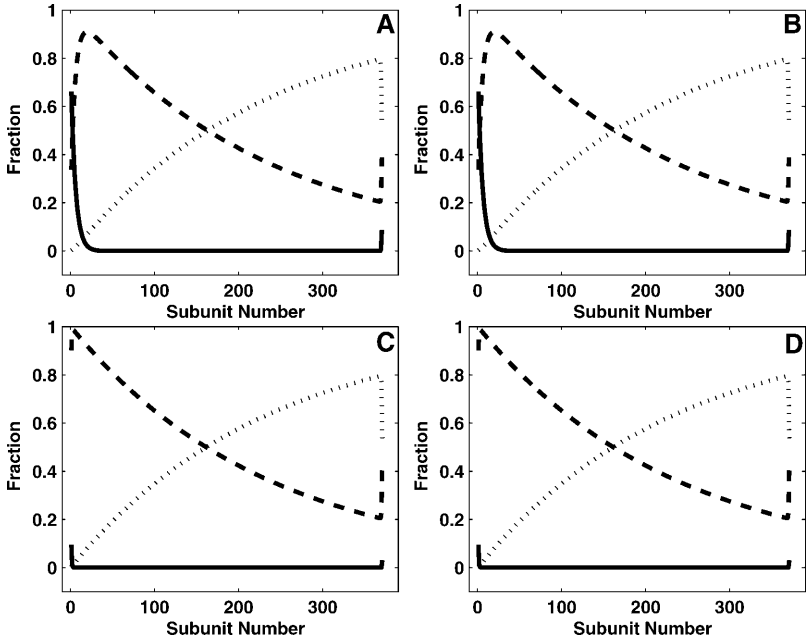

FIGURE 3 Nucleotide profiles in random versus vectorial hydrolysis. Shown are the ATP-bound (*solid lines*), ADP·Pi-bound (*dashed lines*), and ADP-bound (*dotted lines*) subunit fraction profiles from the barbed to the pointed end of 370-subunit (1 μm) filaments, with active cofilin $k_{pD}^{-} = 1.92$ s^{-1} (this is 6.4 times our baseline of 0.3 s^{-1} and based on Moriyama and Yahara, 1999) and 1 μM profilin. Panels *A* and *B* assume random hydrolysis (as do all other figures). *C* and *D* assume vectorial hydrolysis. Panels *A* and *C* are analytical solutions, whereas *B* and *D* are numerical solutions. Other parameters are $\alpha = 1, \beta = 1, n = \sim 0.01$ μM (adjusted slightly to keep the length constant), and $Atot = 4$ μM.

end (~0.1 μM). Our model exhibits both of these features (Fig. 4 *A*). Reasonably, the model also reports no flux (Fig. 4 *B*) and a complete conversion of barbed-end termini to ADP with capping (Fig. 4 *C*); and enhanced flux (Fig. 4 *B*) and enhanced filament polarity with respect to terminal nucleotides with uncapping (Figs. 4, *C* and *D*).

It is somewhat surprising that ADP-G-actin is abundant when barbed ends are fully exposed in Fig. 4 *A*. In these simulations ADP-G-actin is generated by ADP subunit disassembly at pointed ends (Fig. 4 *D*). We know of no experiments that can clearly confirm or contradict this finding. However, we do note that the amount of ADP-G-actin present at steady state is a strong function of filament concentration (see Fig. 6 and associated text) and so an uncontrolled number of filaments may explain sample-to-sample variation in the extent of depolymerization seen in some capping experiments (Walsh et al., 1984).

Increased filament number results in high ADP-G-actin concentration that is removed with profilin addition

A second observation in steady-state experiments is that solutions with high filament numbers contain amounts of G-actin that exceed all ATP critical concentrations (Pantaloni et al., 1984; Selden et al., 1999). Again our model reproduces this observation (Fig. 5 *A*). Both the G-actin pool and filament termini (Fig. 5, *C* and *D*) are increasingly ADP type as filament concentrations increase, and flux slows significantly (Fig. 5 *B*). At the highest concentration of filaments (100 nM), the system tends toward the ADP equilibrium polymer and the ADP critical monomer concentration of 1.8 μM.

Another experimental observation is that the addition of small amounts of profilin to steady-state solutions with high filament concentrations dramatically lowers G-actin levels to near barbed-end ATP critical concentration (Selden et al., 1999). The addition of profilin in our model also produces this behavior (Fig. 6 *A*). Profilin addition is limited in its capacity to increase flux (Fig. 6 *B*) for reasons we examine below.

TABLE 4 Flux in subunits/s assuming random (R) or vectorial (V) hydrolysis*

	$k_{pD}^{-} = 0.30\ s^{-1}$	$k_{pD}^{-} = 1.92\ s^{-1}$
$Ptot = 1\ \mu M$	0.28 (R†)	1.08 (R)
	0.32 (V‡)	1.10 (V)
$Ptot = 0\ \mu M$	0.17 (R)	0.85 (R)
	0.14 (V)	0.83 (V)

*All calculations are for 370 subunit filaments with $\alpha = 1$, $\beta = 1$.
†Random hydrolysis rate is 0.3 s^{-1} (Blanchoin and Pollard, 2002).
‡Vectorial hydrolysis rates are 12.3 s^{-1} (barbed) and 1.3 s^{-1} (pointed) (Carlier et al., 1987).

The ADP disassembly rate constant limits the unregulated cycle

Increasing the rate constant for ADP disassembly from pointed ends, k_{pD}^{-}, enhances flux more than any other individual mechanism (Fig. 7 *B*), indicating that this value is limiting for the unregulated actin cycle. The increase in ATP-type G-actin and the more dramatic increase in ADP-G-actin (Fig. 7 *A*) are trends seen experimentally when ADF/cofilin is added to steady-state F-actin solutions (Didry et al., 1998), although in the experiments the ADP species is likely ADF/cofilin-ADP-G-actin owing the high affinity of ADF/cofilin for ADP-G-actin (Blanchoin and Pollard, 1998; Carlier et al., 1997). Didry et al. (1998) also demonstrate a higher rate of ATP hydrolysis and exchange of tracer nucleotides on G-actin with the addition of ADF/cofilin, and these bulk turnovers are effectively equated to flux (treadmilling) by the assumptions of the article.

In general we note that flux, turnover, and ATP hydrolysis are not the same quantities. ATP hydrolysis and nucleotide exchange will certainly increase as treadmilling increases, but they can also rise from an increased number of filaments (ATPases) even as the flux through individual filaments declines. In addition, even though flux and turnover must be essentially zero for filaments that are fully capped, the ATP consumption rate will be nonzero since ATP-G-actin can add to the pointed end, hydrolyze, and fall off.

We observe that the capacity of enhanced ADP disassembly to increase flux is limited (Fig. 7 *B*). The limitation apparently comes from the depletion of ADP subunits from the pointed ends of filaments (Fig. 7 *D*) so that the disassembly is restricted not by the rate constant k_{pD}^{-} but by the product of k_{pD}^{-} and the number of ADP-terminated pointed ends.

Profilin and enhanced ADP disassembly combine to increase flux

In seeking the maximum flux that could be achieved through a combination of mechanisms, we initially excluded the mechanism of enhanced Pi release. With this restriction we found that only the addition of profilin could enhance the flux beyond the 2.1 subunits/s rate seen with enhanced ADP disassembly alone (Fig. 8). A maximum flux of 2.6 subunits/s was calculated for 4 μM actin when the concentration of filaments is 0.002 μM, $k_{pD}^{-} = 10\ s^{-1}$, total profilin = 1 μM, and all ends are exposed. Increasing the number of filaments, capping pointed or barbed ends, or adding β_4-thymosin equimolar with actin, only slowed subunit flux.

Synergy between profilin and accelerated ADP subunit disassembly in enhancing actin dynamics at steady state is consistent with experimental data (Didry et al., 1998), but the increase in flux (~25%) with added profilin we found here is

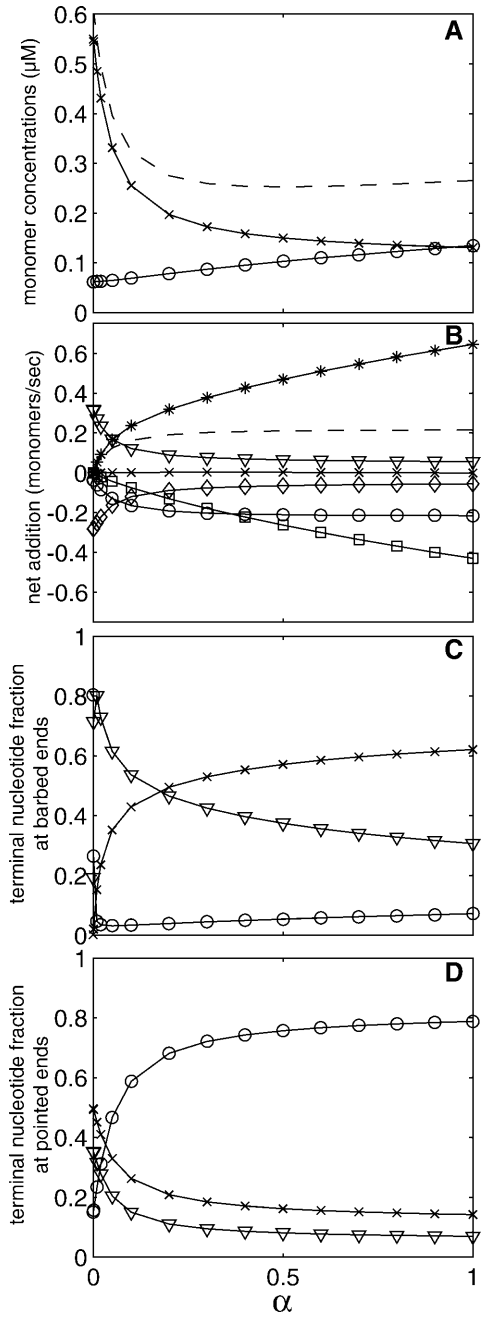

FIGURE 4 Effects of barbed end capping. (*A*) Effects on G-actin concentrations. Full capping of barbed ends ($\alpha = 0$) increases the amount of total monomer (*dashed line*) to the pointed-end ATP critical concentration, but ADP (○) monomers are still present. (*B*) Effects on assembly and flux. Uncapped filaments predominantly add ATP-type-actin at the barbed end (*), and lose ADP subunits (○) from the pointed end and ADP·Pi (□) subunits from the barbed end. Capping >90% sharply reduces the flux (*dashed line*). (*C* and *D*) Effects on terminal nucleotide identity. (*C*) Barbed ends: slightly uncapped barbed ends are predominantly ADP·Pi bound (▽), and the fraction that are ATP (×) bound rise quickly with further uncapping. (*D*) Pointed ends: capping changes the pointed end from mostly ADP (○) to mostly ATP (×) and ADP·Pi (▽). In all panels, α ranges from .0001 to 1. Symbols for Figs. 4–7, 9, and 10: (*A*) G-actin with ATP (×) or ADP (○), profilin-actin with ATP (▽) or ADP (*). Total G-actin (*dashed lines*). (*B*) Net addition or loss at the barbed end via ATP (*), ADP·Pi (□), ADP, (×) or pointed end: ATP (▽), ADP·Pi (◇), ADP (○). Total flux (*dashed lines*). (*C* and *D*) ATP (×), ADP·Pi (▽), ADP (○). When not specified, the basic parameters are set at $\alpha = 1$, $\beta = 1$, $Ptot = 0$ μM, $Btot = 0$ μM, $Atot = 4$ μM, $n = 0.002$ μM, $k_{pD}^{-} = 0.3$ s^{-1}, and $k_{fD\cdot Pi\rightarrow D} = 0.0026$ s^{-1}.

relatively modest. Also, the overall rate of flux is limited to a value that is too small to account for the smallest turnover times (~30 s) reported in cells (Theriot and Mitchison, 1991). Assuming these turnover values derive from ~0.5 μm filaments, our model appears limited to a flux ~twofold smaller than cells can achieve. Examining the details of the cycle at the maximum flux reveals that the depletion of ADP at pointed ends still limits the cycle (Fig. 9 *D*) as in the case of enhanced ADP subunit disassembly alone (Fig. 7 *D*). Apparently the addition of profilin primarily recharges and polymerizes the large ADP-G-actin pool that accumulates with the enhanced ADP subunit disassembly (compare Fig. 7 *A* and Fig. 9 *A*). It also aids the flux by lengthening filaments so that the age of the subunits that arrive at the pointed ends is greater and slightly more have converted to ADP (compare Fig. 7 *D* and Fig. 9 *D*).

Pi release becomes rate limiting at high rates of ADP subunit off rates

We reasoned that if the depletion of ADP-termini at pointed ends is ultimately limiting for flux, then increasing the rate of Pi release on filaments should restore these termini and overcome the limitation. We confirmed this idea in simulations that increased the rate of Pi release on filaments, $k_{fD\cdot Pi\rightarrow D}$, 15-fold from the unregulated value of 0.0026 s^{-1} (Fig. 10). Under these conditions (also 4 μM actin, 0.002 μM filaments, 1 μM profilin, $k_{pD}^{-} = 10s^{-1}$), the flux rises to 5.5 subunits/s (Fig. 10 *B*), which is close to the rate that cells may achieve. Like increased ADP disassembly, increased Pi release follows from ADF/cofilin binding to filaments (Blanchoin and Pollard, 1999), and so our analysis demonstrates how these two functions of ADF/cofilin work together to increase flux.

It is interesting to note that the flux has again plateaued with higher Pi release rates (Fig. 10 *B*). The limit can apparently be blamed on a limited ability of Pi release to create ADP pointed ends (Fig. 10 *D*), only unlike the case before $k_{fD\cdot Pi\rightarrow D}$ was elevated (Fig. 9 *D*), ATP subunits rather than ADP·Pi subunits rise to compete for the terminal position on pointed ends. The enhancement of disassembly and Pi release in this simulation causes depolymerization but filaments are still ~1500 subunits long and so these ATP subunits cannot be arriving from the barbed end. Instead we see that profilin's ability to direct ATP-G-actin to barbed ends is limited. Some of the increasing free ATP-G-actin species assembles at the pointed ends and reduces the space for ADP subunits.

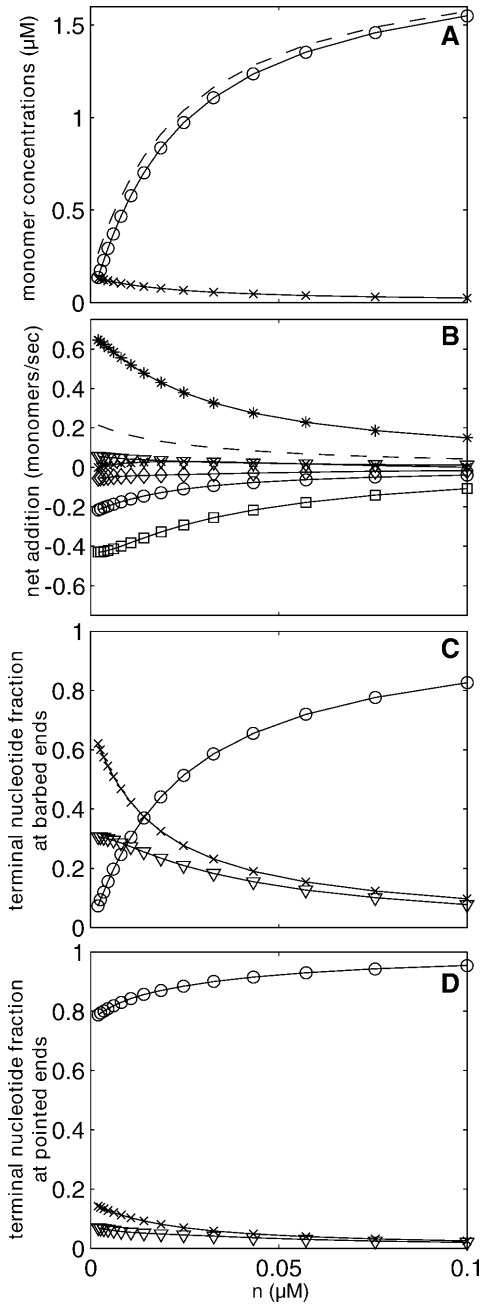

FIGURE 5 Effects of increased filament number. (*A*) Effects on G-actin concentrations. Increasing filament number dramatically increases the amount of ADP (○) monomer, decreasing the amount of ATP (×) monomer. (*B*) Effects on assembly and flux. Increasing filament number decreases flux (*dashed line*). (*C* and *D*) Effects on terminal nucleotide identity*:* (*C*) Barbed end: increasing filament number increases the fraction of barbed ends bound to ADP (○). (*D*) Pointed end: increasing filament number has minimal effects at the pointed end. Filament concentration, *n*, varies from 0.002 to 0.1 μM in all panels. See Fig. 4 legend for unmentioned symbols and standard parameter values.

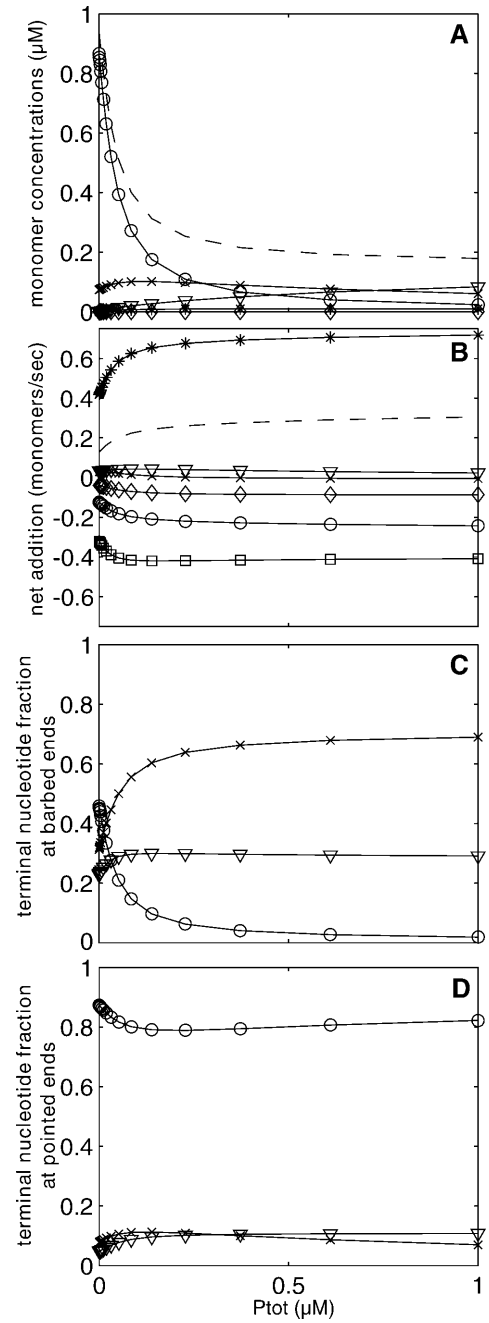

FIGURE 6 Effects of profilin with elevated filament number. (*A*) Effects on G-actin concentrations. Nanomolar profilin causes a significant drop in monomer total monomer concentration (*dashed line*), primarily by binding ADP-G-actin (○) and converting it to ATP-G-actin (×), which adds to the barbed end. Addition of more profilin changes the most abundant monomer species to profilin-ATP-G-actin complex (▽). (*B*) Effects on assembly and flux. Profilin addition increases the flux (*dashed line*) slightly, but the effect rapidly plateaus. (*C* and *D*) Effects on terminal nucleotide identity*:* (*C*) Barbed ends: profilin eliminates ADP-termini (○) and creates ATP-termini (×). (*D*) Pointed ends: profilin has only small effects, slightly raising the ADP·Pi fraction (▽) and slightly decreasing the ADP fraction (○). Profilin varies from 0 to 1 μM and $n = 0.020$ μM in all panels. The effects of profilin are similar for $n = 0.002$ μM. See Fig. 4 legend for unmentioned symbols and standard parameter values.

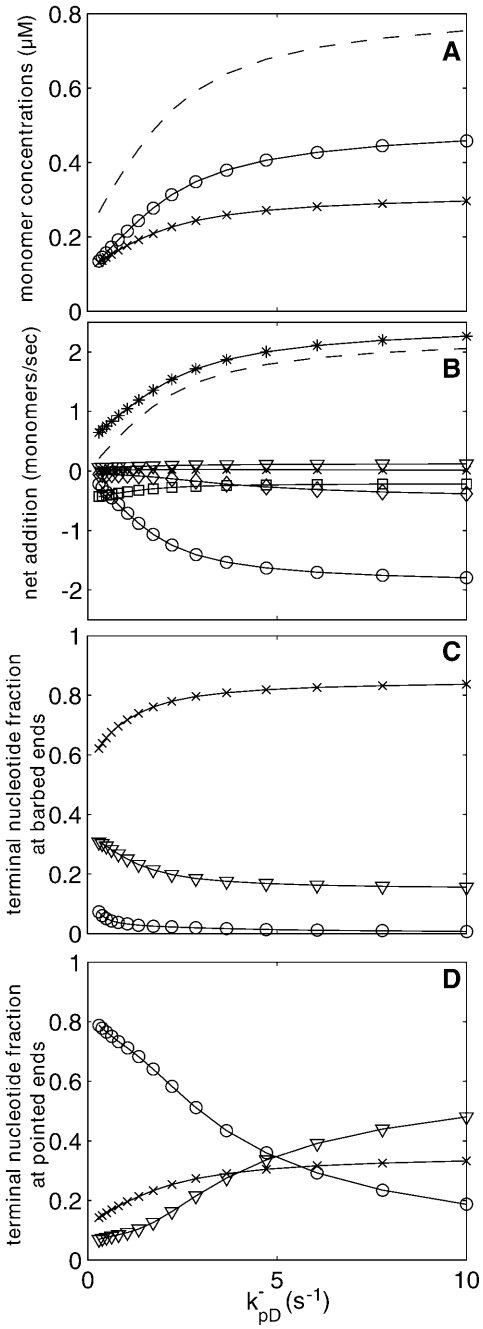

FIGURE 7 Effects of increasing ADP disassembly rate constants. (*A*) Effects on G-actin concentrations. The larger off rates cause a rise in the total monomer concentration (*dashed line*) mostly due to a rise in ADP-G-actin (○), but ATP-G-actin (×) also rises. (*B*) Effects on assembly and flux. Flux (*dashed line*) significantly increases, identifying k_{pD}^- as rate-limiting for unregulated filaments. (*C* and *D*) Effects on terminal nucleotide identity*:* (*C*) Barbed end. (*D*) Pointed end: pointed ends transition from mostly ADP (○) to mostly ADP·Pi (▽) and ATP (×). In all panels, k_{pD}^- varies from 0.3 to 10 s^{-1} . See Fig. 4 legend for unmentioned symbol definitions and standard parameter values. Note that k_{bD}^- varies as k_{pD}^- varies (see ''Mathematical Model'').

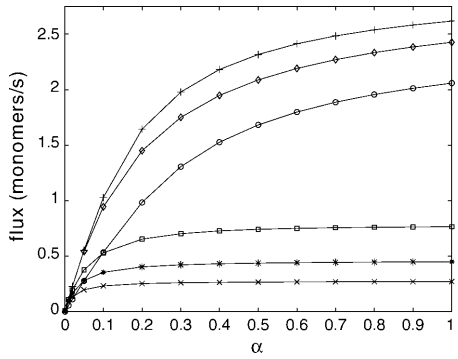

FIGURE 8 Combining regulated mechanisms to achieve a maximal flux. The combination of higher ADP off rates ($k_{pD}^- = 10$ s^{-1}) and profilin (1 μM) gives the highest flux (+) with other parameters at standard values (see Fig. 4 legend). Other curves are: added β_4-thymosin (◇) (*Btot* = 4 μM), removed profilin (○) (*Ptot* = 0 μM), increased filament number (□) ($n = 0.1$ μM), unregulated ADP subunit off-rates (*) ($k_{pD}^- = 0.3$ s^{-1}), and capping pointed ends 95% (×) ($\beta = .05$). Uncapping barbed ends occurs for all curves from left to right.

A complex interplay exists between profilin and mechanisms for ADP disassembly and Pi release

Our results indicate that profilin concentration, and mechanisms for ADP disassembly and Pi release, all have roles in limiting the flux, although the explanation always reduces to some restriction on the product of k_{pD}^- and $g_{pD(1)}$. In Fig. 11, we examine the interplay between these mechanisms more systematically. Beginning with barbed end uncapping so that our baseline flux is zero, we turn on individual mechanisms that enhance flux and monitor both flux and filament length. Fig. 11 *A* shows a behavior similar to that described in the progression of figures above: enhancing k_{pD}^- provides a more significant boost in flux rate than the subsequent introduction of profilin, but the system is clearly limited by inability to release Pi. The remarkable boost in flux to >13 subunits/s is a product of the exaggerated values for all three mechanisms (100 × for the rates and > 2 × equimolar with total actin for profilin). This can be appreciated by reversing the order of application of profilin and enhanced Pi release to again dramatically arrive at 13 subunits/s flux only with the addition of the last mechanism (Fig. 11 *B*). The dash-dotted line in both panels shows the effects of 100 × nucleotide exchange with no profilin, and so the distance to the solid line illustrates the importance of profilin's capacity to direct ATP-G-actin to barbed ends. At the maximum flux in these figures, ADP disassembly can be further increased, followed by the increases in the other mechanisms, and the flux rates will continue to climb. Such cycles can't be repeated indefinitely because profilin eventually loses the battle to maintain polymerized filaments.

DISCUSSION

We have developed a broad mathematical model of the steady-state dynamics of purified actin that includes its key

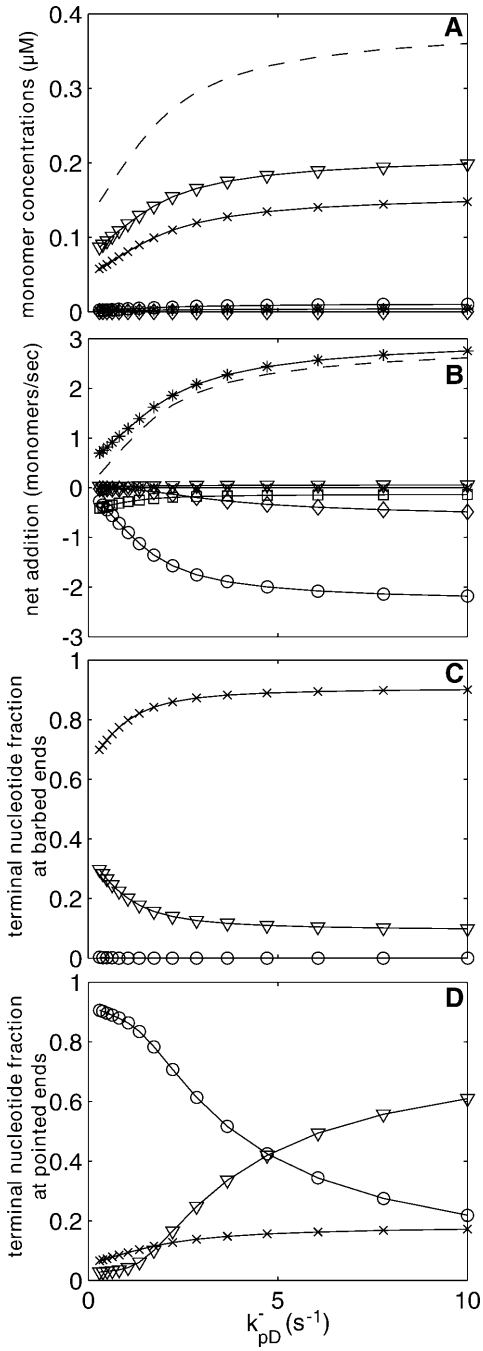

FIGURE 9 Details of the cycle at the apparent maximal flux. In all panels, $Ptot = 1$ μM. (*A*) G-actin concentrations. The presence of profilin significantly decreases rise in monomer concentration (*dashed line*) compared to elevated ADP off rates alone (compare to Fig. 7). (*B*) Assembly and flux. The presence of profilin increases the maximal flux (*dashed line*) compared to elevated ADP off rates alone. (*C* and *D*) Terminal nucleotide identities: (*C*) Barbed end: profilin slightly increases the ATP fraction ($\times$). (*D*) Pointed end: termini identities are similar to those without profilin except the ATP fraction ($\times$) is lower. See Fig. 4 legend for unmentioned symbol definitions and standard parameter values.

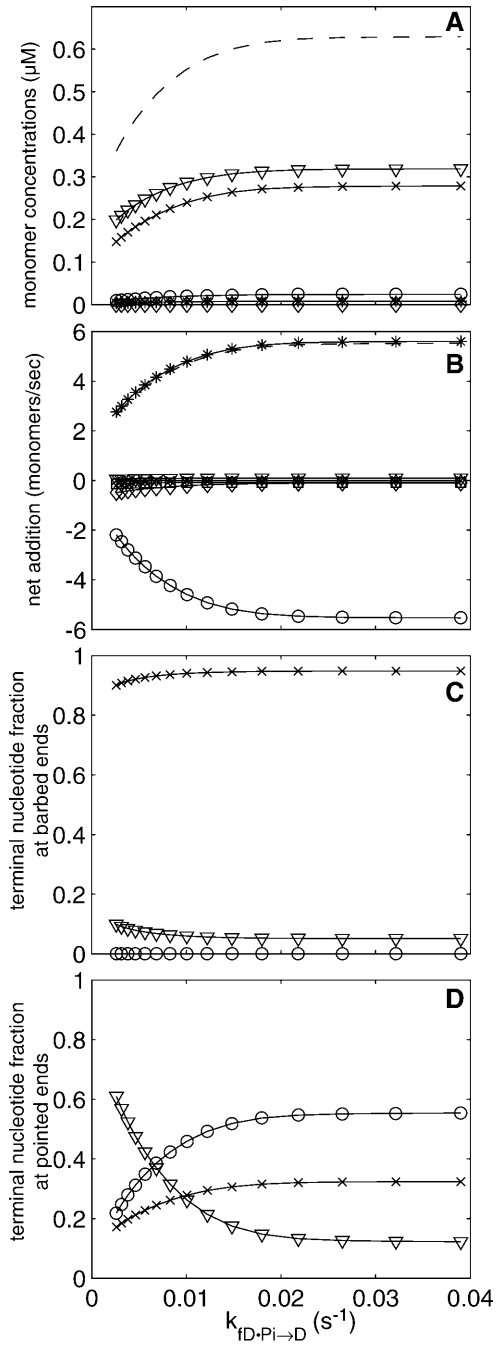

FIGURE 10 Pi release rate is limiting for further increases in flux. Starting from the conditions that produce maximal flux ($k^-_{pD} = 10$ s^{-1}, $Ptot = 1$ μM, $\alpha = 1$), increasing the Pi release rate on filaments 15-fold from .0026 to .039 s^{-1} increases maximal flux ~twofold (*B*). It also increases the amount of unpolymerized actin and decreases the ADP·Pi content at both barbed and pointed ends. See Fig. 4 legend for unmentioned symbol definitions and standard parameter values.

modes of regulation. We modeled profilin explicitly, because the understanding of profilin's multiple connected functions and their associated rates appears to have reached a reasonable consensus. The other mechanisms—increased filament number, elevated rate constants for ADP subunit disassem-

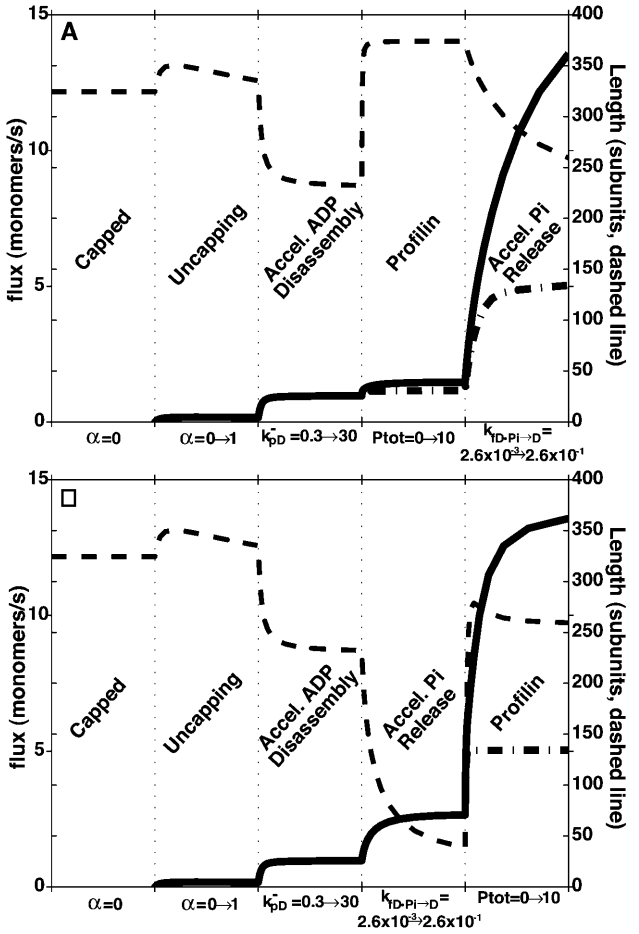

FIGURE 11 Sequential removal of barriers to flux. (*A*) Parameters are changed in a sequence similar to the sequence of previous figures (4 μM actin, 10 nM filaments). (*B*) The order of profilin addition and enhanced Pi release are reversed. Symbols: solid line, flux; dashed line, corresponding filament length *(right axis)*; and dash-dotted line, no profilin but 100× nucleotide exchange (i.e., profilin without its barbed-end shuttle feature). The figure illustrates that the Pi release rate, ADP subunit off rates, and the level of profilin are all essential to determining the system flux; an arbitrary limit on any one of these limits the entire system. In theory only, the rate constants can be arbitrarily increased to enhance flux until the capacity of profilin to maintain the polymer is overcome. Unspecified conditions are 4 μM actin, 10 nM filaments, $Btot = 0$, and $\beta = 1$.

bly, enhanced rate of Pi release, and barbed- and pointed-end capping—are known points of regulation in the actin cycle (Fig. 1). Our model therefore implicitly represents proteins with these activities and often artificially separates what are actually multiple and connected functions.

Our primary advance over all previous models is the solution to the complete nucleotide profile within filaments. We have achieved this solution numerically and analytically and for the competing theories of vectorial and random hydrolysis of ATP in filaments. Our numerical and analytical solutions agree completely. The agreement provides an important check on our work and supports the idea that the complex system of equations has only one reasonable solution.

The solution to the nucleotide profile is useful for several reasons. First, it represents an important breakthrough for interpreting complex experiments on steady-state actin. Experimentalists frequently need to estimate the nucleotide content of filament ends to interpret data because these ends determine both the dynamics of filaments and the nucleotide composition of the G-actin pool. Because of the complexity of the calculation, the estimates involve simplifications that may compromise the interpretation of data. Our analytical solutions to the filament composition (see Appendix) should now be used for these experiments, even with models that differ from ours with respect to the dynamics of G-actin.

A second reason our solution is significant is that the nucleotide profile determines network geometries and dynamics by controlling where certain regulatory proteins bind and unbind along filaments. With ATP-G-actin addition occurring primarily at filament barbed ends and hydrolysis and Pi release following in serial fashion, the nucleotide state of a subunit suggests its age and, to a lesser degree, its proximity to the barbed end. By specifically binding to ADP containing subunits (Carlier et al., 1997), ADF/cofilin molecules select the oldest regions of filaments for disassembly, and these regions tend to be closer to the pointed end. By contrast, filament branches nucleated by Arp2/3 complex appear to favor the ATP/ADP·Pi state of filaments and debranch upon Pi release (Blanchoin et al., 2000). In these ways the nucleotide profile converts the polarity of individual filaments into the orientation of a large treadmilling network thought to operate at the leading edge of motile cells (Pollard et al., 2000). Our solutions should be used in future steady-state models that seek to explicitly represent the binding of ADF/cofilins and Arp2/3 complex to predict network geometry and dynamics.

An intriguing question that arose in our work concerns the transition between the equilibrium and dynamic actin polymers. Thermodynamically, a filament bound exclusively to either ATP, ADP·Pi, or ADP interacting with monomers of the same type is at true equilibrium, and therefore the critical concentrations at both ends must be equal. Consequently, energetic differences between ATP/ADP conformations must loosely explain how treadmilling filaments maintain different critical concentrations at their ends. This also means that at least some kinetic constants must change between the equilibrium and nonequilibrium polymers, and that these changing constants must be some continuous function of the nucleotide composition. It would be fascinating if experimentalists attempted to resolve the rate constant transitions, perhaps using nonhydrolyzable ATP and inorganic phosphate to establish the equilibrium polymers. Our solution for the nucleotide profile or a modified version that included all equilibrium polymers could assist the effort.

Our model reproduces numerous behaviors seen in actin solutions, including experiments with capping proteins,

profilin, ADF/cofilin, and those that vary filament number through sonication. The qualitative agreement with these experiments is very good. The quantitative agreement is good enough that it becomes difficult to decide if disparities should motivate changes in the model or refined experiments. The difficulty is that no experiment directly controls or measures all model parameters. An example is our model's prediction that the most abundant species of monomer for unregulated 4 μM actin with >0.002 μM filaments is ADP-G-actin (Fig. 5). One experimental approach to distinguishing ADP and ATP-type monomer employs β_4-thymosin to selectively bind ATP-type monomer (Didry et al., 1998), but the particular studies we might compare to do not estimate filament number, which is an important determinant of the amount of ADP-G-actin for unregulated actin.

Certainly the model must be quantitatively inaccurate in some respects because it required simplifications and assumptions. Some inaccuracy must derive, for example, from our simplification that filaments are all the same length. Actual lengths are distributed exponentially (Sept et al., 1999), and the dynamics of short and long filaments in such mixtures should be different.

We used our model to examine the importance of various mechanisms in determining the rate of subunit flux through filaments. Beginning with unregulated filaments, we found that elevating the rate constant for the off rate of ADP subunits from pointed ends had the strongest impact on flux (at 4 μM actin and 0.002 μM filaments) and that profilin addition increased flux slightly. In combination, both mechanisms were limited to a flux of $\sim$2.6 subunits/s, which cells apparently exceed.

Examining concentrations in the maximized cycle, we discovered that few pointed-end termini were still bound to ADP ($g_{\mathrm{pD}(1)} \rightarrow 0$). This explained why elevating the constant k_{pD}^{-} eventually became futile: the product of k_{pD}^{-} and $g_{\mathrm{pD}(1)}$ had approached some limit. It also suggested that elevating Pi release ($k_{\mathrm{fD{\cdot}Pi}\rightarrow\mathrm{D}}$) on filaments to increase $g_{\mathrm{pD}(1)}$ would further enhance the flux. Increasing the rate of Pi release 15-fold did raise the flux to $\sim$5.5 subunits/s, a level near high estimates from cells. This result gives a new appreciation for how two of the functions of ADF/cofilin work together to drive the actin cycle toward higher flux rates.

In the above analysis, we increased k_{pD}^{-} and $k_{\mathrm{fD{\cdot}Pi}\rightarrow\mathrm{D}}$ arbitrarily to maximize flux. We now note that a $>$10-fold increase in $k_{\mathrm{fD{\cdot}Pi}\rightarrow\mathrm{D}}$ by cofilin binding has been reported in the literature (Blanchoin and Pollard, 1999). Estimates for the extent that k_{pD}^{-} may increase with ADF/cofilin range from a lower estimate of 6.4-fold (Moriyama and Yahara, 1999) to values of 25- (Carlier et al., 1997) and 50-fold (Didry et al., 1998). The higher values are controversial because of difficulties in separating severing contributions to bulk turnover measurements. The lower value was determined using a method that simultaneously estimated severing and off rate, but was measured for substoichiometric quantities of cofilin and so it may not represent a maximum. We can only note that for the simulations producing $\sim$5 subunits/s flux, the maximum k_{pD}^{-} of 10 s^{-1} falls within the range of the literature reports (it is an $\sim$30-fold increase).

Our experience made us curious about the limits on flux that derive from arbitrary limits placed on profilin level, the ADP disassembly rate k_{pD}^{-}, or the Pi release rate on filaments $k_{\mathrm{fD{\cdot}Pi}\rightarrow\mathrm{D}}$. Disregarding what limits nature may prescribe for these mechanisms, we increased their values until their effects on the flux fully saturated. Importantly, the order in which the three mechanisms are applied is not important so long as all three are eventually applied (Fig. 11). Thus each mechanism makes some unique and essential contribution to the flux.

Examining concentrations in detail provides simplifying concepts for thinking about the steady-state actin cycle. One can imagine the bottleneck for the steady-state actin cycle is the product of the ADP pointed-end disassembly rate and the number of ADP-bound pointed end termini ($k_{\mathrm{pD}}^{-} \times g_{\mathrm{pD}(1)}$), and either factor in the product can be limiting. Under conditions where there are numerous ADP pointed-end termini, the rate constant k_{pD}^{-} can be increased to increase flux, until eventually the ADP pointed ends are depleted. Once $g_{\mathrm{pD}(1)}$ is low, either $g_{\mathrm{pT}(1)}$, $g_{\mathrm{pD{\cdot}Pi}(1)}$, or both, must be high. If $g_{\mathrm{pT}(1)}$ is high, it is because significant ATP-G-actin is assembling at pointed ends, and more profilin can be introduced to divert this population to barbed ends. Similarly, if $g_{\mathrm{pD{\cdot}Pi}(1)}$ is high, it is because many subunits are arriving at the pointed end before Pi release can occur, and so increasing Pi release provides a remedy. In this way, each of the three mechanisms specifically eliminates one of three unique barriers to flux. Remarkably, in our theoretical study there are no other barriers other than the total amount of actin. The simulations show a trend, slowed but not stopped by profilin, where increased flux leads to less polymerized actin.

APPENDIX: ANALYTICAL SOLUTION TO THE NUCLEOTIDE PROFILE IN FILAMENTS

The case of random ATP hydrolysis

We begin by considering the ADP·Pi profile within filaments. Analogous to Eqs. M11–M14 (Table 3), we require no net production of ADP·Pi at internal subunits at steady state with

$$0 = k_{\mathrm{e,\,ON}}\left(g_{\mathrm{eD{\cdot}Pi}(\mathrm{i}-1)} - g_{\mathrm{eD{\cdot}Pi}(\mathrm{i})}\right) + k_{\mathrm{e,\,OFF}}\left(g_{\mathrm{eD{\cdot}Pi}(\mathrm{i}+1)} - g_{\mathrm{eD{\cdot}Pi}(\mathrm{i})}\right) - k_{\mathrm{fD{\cdot}Pi}\rightarrow\mathrm{D}}g_{\mathrm{eD{\cdot}Pi}(\mathrm{i})} + k_{\mathrm{T}\rightarrow\mathrm{D{\cdot}Pi}}g_{\mathrm{eT}(\mathrm{i})}, \quad \text{(A1)}$$

where $k_{\mathrm{e,\,ON}} = \gamma(k_{\mathrm{eT}}^{+}([at] + \zeta[Pat]) + k_{\mathrm{eD{\cdot}Pi}}^{+}([adpi] + \zeta[Padpi]) + k_{\mathrm{eD}}^{+}([ad] + \zeta[Pad]))$, $k_{\mathrm{e,\,OFF}} = \gamma(k_{\mathrm{eT}}^{-}g_{\mathrm{eT}(1)} + k_{\mathrm{eD{\cdot}Pi}}^{-}g_{\mathrm{eD{\cdot}Pi}(1)} + k_{\mathrm{eD}}^{-}g_{\mathrm{eD}(1)})$, $\gamma = \alpha$ and $\zeta = 1$ when $e = b$ (barbed end) or $\gamma = \beta$ and $\zeta = 0$ when $e = p$ (pointed end). Equation A1 is a second-order linear nonhomogeneous difference equation in $g_{\mathrm{eD{\cdot}Pi}(\mathrm{i})}$ with constant coefficients. The corresponding homogeneous equation is

$$0 = k_{\mathrm{e,\,ON}}\left(g_{\mathrm{eD{\cdot}Pi}(\mathrm{i}-1)} - g_{\mathrm{eD{\cdot}Pi}(\mathrm{i})}\right) + k_{\mathrm{e,\,OFF}}\left(g_{\mathrm{eD{\cdot}Pi}(\mathrm{i}+1)} - g_{\mathrm{eD{\cdot}Pi}(\mathrm{i})}\right) - k_{\mathrm{fD{\cdot}Pi}\rightarrow\mathrm{D}}g_{\mathrm{eD{\cdot}Pi}(\mathrm{i})}. \quad \text{(A2)}$$

Trying a solution of the form $g_{eD\cdot Pi(i)} = \delta_e^i$ gives

$$0 = k_{e,OFF}\delta_e^{i+1} - (k_{e,OFF} + k_{e,ON} + k_{fD\cdot Pi\to D})\delta_e^i + k_{e,ON}\delta_e^{i-1}. \quad (A3)$$

Provided $\delta_e \neq 0$, we divide by δ_e^{i-1} to give

$$0 = k_{e,OFF}\delta_e^2 - (k_{e,OFF} + k_{e,ON} + k_{fD\cdot Pi\to D})\delta_e + k_{e,ON}. \quad (A4)$$

Solving for the roots gives

$$\delta_e^{\pm} = \frac{k_{e,OFF} + k_{e,ON} + k_{fD\cdot Pi\to D}}{2k_{e,OFF}} \pm \frac{\sqrt{(k_{e,OFF} + k_{e,ON} + k_{fD\cdot Pi\to D})^2 - 4k_{e,OFF}k_{e,ON}}}{2k_{e,OFF}}. \quad (A5)$$

Given that all rate constants, concentrations, and subunit fractions are positive, both roots are real and positive with $\delta_e^+ > 1$ and $\delta_e^- < 1$. The general solution to the homogeneous problem (which we denote $g_{eD\cdot Pi(i),H}$) is the linear combination of the two solutions

$$g_{eD\cdot Pi(i),H} = A_e(\delta_e^+)^i + B_e(\delta_e^-)^i, \quad (A6)$$

where A_e and B_e are arbitrary constants to be determined from boundary conditions.

To arrive at a complete solution, we first note that the nonhomogeneous term in Eq. A1 is the term $k_{T\to D\cdot Pi}\, g_{eT(i)}$. Because the usual procedure is to guess a particular solution based on the form of the nonhomogeneous term, we are compelled to first find the solution to $g_{eT(i)}$. In the case of random ATP hydrolysis, the equation governing the ATP profile is

$$0 = k_{e,ON}(g_{eT(i-1)} - g_{eT(i)}) + k_{e,OFF}(g_{eT(i+1)} - g_{eT(i)}) - k_{fD\cdot Pi\to D}g_{eT(i)}. \quad (A7)$$

This equation is analogous to Eq. A1, but without the nonhomogeneous term, since there is no source of ATP subunits other than polymerization. The general solution to the ATP profile in the case of random hydrolysis is therefore

$$g_{eT(i)} = C_e(\lambda_e^+)^i + D_e(\lambda_e^-)^i, \quad (A8)$$

where λ_e^+ and λ_e^- are determined from Eq. A5 only with $k_{T\to D\cdot Pi}$ replacing $k_{fD\cdot Pi\to D}$ (thus $\lambda_e^+ \neq \delta_e^+$), and C_e and D_e are constants to be determined from boundary conditions.

Since Eq. A8 has two linearly independent components, we can construct two particular solutions to the ADP·Pi profile in the form $N_1 = E_e(\lambda_e^+)^i$ and $N_2 = F_e(\lambda_e^-)^i$. The constants E_e and F_e are found from substituting these solutions into Eq. A1 along with the corresponding component from Eq. A8:

$$E_e = \frac{-k_{T\to D\cdot Pi}C_e\lambda_e^+}{k_{e,OFF}(\lambda_e^+)^2 - (k_{e,OFF} + k_{e,ON} + k_{fD\cdot Pi\to D})\lambda_e^+ + k_{e,ON}} \quad (A9)$$

$$F_e = \frac{-k_{T\to D\cdot Pi}D_e\lambda_e^-}{k_{e,OFF}(\lambda_e^-)^2 - (k_{e,OFF} + k_{e,ON} + k_{fD\cdot Pi\to D})\lambda_e^- + k_{e,ON}}. \quad (A10)$$

The complete solution to the ADP·Pi profile is the sum of the homogeneous and particular solutions $g_{eD\cdot Pi(i)} = g_{eD\cdot Pi(i),H} + N_1 + N_2$ or

$$g_{eD\cdot Pi(i)} = A_e(\delta_e^+)^i + B_e(\delta_e^-)^i + E_e(\lambda_e^+)^i + F_e(\lambda_e^-)^i. \quad (A11)$$

Equations A8 and A11 represent a complete solution to the nucleotide profiles inside the filaments for the case of random ATP hydrolysis. Note that there are four equations as $e = b$ is the barbed-end solution and $e = p$ is the pointed-end solution. The eight constants A_b, B_b, A_p, B_p, C_b, D_b, C_p, and D_p are determined at the boundaries as follows. First we require that the fractions at the termini connect to the interior positions

$$g_{eT(1)} = C_e\lambda_e^+ + D_e\lambda_e^- \quad (A12)$$

$$g_{eD\cdot Pi(1)} = A_e\delta_e^+ + B_e\delta_e^- + E_e\lambda_e^+ + F_e\lambda_e^-. \quad (A13)$$

Then we require that the pointed- and barbed-end solutions have both the same value and the same slope in the center of the filament:

$$g_{bT(i^*)} = g_{pT(i^*)} \quad (A14)$$

$$g_{bD\cdot Pi(i^*)} = g_{pD\cdot Pi(i^*)} \quad (A15)$$

$$\frac{d}{di}g_{bT(i^*)} = \frac{d}{di}g_{pT(i^*)} \quad (A16)$$

$$\frac{d}{di}g_{bD\cdot Pi(i^*)} = \frac{d}{di}g_{pD\cdot Pi(i^*)}, \quad (A17)$$

where i^* is either an actual subunit centered between the two filament halves or a virtual subunit in the case of filaments with an even number of subunits.

The case of vectorial ATP hydrolysis

In the case of vectorial ATP hydrolysis, we have found no analytical solution to the ATP profile and therefore we cannot treat the heterogeneity in Eq. A1 for the ADP·Pi profile. Thus we solve the ATP profile numerically until we reach an ATP-free ''core'' within the filament. At this point the homogeneous problem in Eq. A2 applies for the ADP·Pi profile and the solution is Eq. A6. The boundary conditions Eqs. A13, A15, and A17 are applied as for the random hydrolysis model, only the ADP·Pi profile doesn't begin at the terminal filament subunit but 10 subunits interior from the terminal. In all simulations, this has proved to be a conservative estimate of where the ATP-free core begins for the rate constants used.

The actin cycle model is accessible to all readers through an interactive web page at *http://mcgrathlab.urmc.rochester.edu/ActinCycle/*.

The authors are indebted to an anonymous reviewer whose comments helped us navigate the field's rich history and the wide array of possible assumptions. Thanks to Prof. Mike King and Catherine Howell for helpful comments on the text.

This work was supported by University of Rochester start-up money.

REFERENCES

Ballweber, E., E. Hannappel, T. Huff, H. Stephan, M. Haener, N. Taschner, D. Stoffler, U. Aebi, and H. G. Mannherz. 2002. Polymerisation of chemically cross-linked actin:thymosin β_4 complex to filamentous actin: alteration in helical parameters and visualisation of thymosin β_4 binding on F-actin. *J. Mol. Biol.* 315:613–625.

Blanchoin, L., and T. D. Pollard. 1998. Interaction of actin monomers with Acanthamoeba actophorin (ADF/cofilin) and profilin. *J. Biol. Chem.* 273:25106–25111.

Blanchoin, L., and T. D. Pollard. 1999. Mechanism of interaction of Acanthamoeba actophorin (ADF/cofilin) with actin filaments. *J. Biol. Chem.* 274:15538–15546.

Blanchoin, L., and T. D. Pollard. 2002. Hydrolysis of ATP by polymerized actin depends on the bound divalent cation but not profilin. *Biochemistry.* 41:597–602.

Blanchoin, L., T. D. Pollard, and R. D. Mullins. 2000. Interactions of ADF/cofilin, Arp2/3 complex, capping protein and profilin in remodeling of branched actin filament networks. *Curr. Biol.* 10:1273–1282.

Brenner, S. L., and E. D. Korn. 1980. The effects of cytochalasins on actin polymerization and actin ATPase provide insights into the mechanism of polymerization. *J. Biol. Chem.* 255:841–844.

Burt, C. T., T. Glonek, and M. Barany. 1977. Analysis of living tissue by phosphorus-31 magnetic resonance. *Science.* 195:145–149.

Carlier, M. F., D. Didry, I. Erk, J. Lepault, M. Van Troys, J. Vanderkerckhove, I. Perelroizen, H. Yin, Y. Doi, and D. Pantaloni. 1996. T-β4 is not a simple G-actin sequestering protein and interacts with F-actin at high concentration. *J. Biol. Chem.* 271:9231–9239.

Carlier, M. F., C. Jean, K. Rieger, M. Lenfant, and D. Pantaloni. 1993. Modulation of the interaction between G-actin and thymosin β4 by the ATP/ADP ratio: possible implication in the regulation of actin dynamics. *Proc. Natl. Acad. Sci. USA.* 90:5034–5038.

Carlier, M. F., V. Laurent, J. Santolini, R. Melki, D. Didry, G.-X. Xia, Y. Hong, N.-H. Chua, and D. Pantaloni. 1997. Actin depolymerizing factor (ADF/cofilin) enhances the rate of filament turnover: implication in actin based motility. *J. Cell Biol.* 136:1307–1322.

Carlier, M. F., and D. Pantaloni. 1986. Direct evidence for ADP-Pi-F-actin as the major intermediate in ATP-actin polymerization. Rate of dissociation of Pi from actin filaments. *Biochemistry.* 25:7789–7792.

Carlier, M. F., D. Pantaloni, and E. Korn. 1987. The mechanisms of ATP hydrolysis accompanying the polymerization of Mg-actin and Ca-actin. *J. Biol. Chem.* 262:3052–3059.

Carlsson, A. E. 2001. Growth of branched actin networks against obstacles. *Biophys. J.* 81:1907–1923.

Didry, D., M. F. Carlier, and D. Pantaloni. 1998. Synergy between actin depolymerizing factor/cofilin and profilin in increasing actin filament turnover. *J. Biol. Chem.* 273:25602–25611.

Dufort, P., and C. Lumsden. 1996. How profilin/barbed-end synergy controls actin polymerization: a kinetic model of the ATP hydrolysis circuit. *Cell Motil. Cytoskeleton.* 35:309–330.

Fujiwara, I., S. Takahashi, H. Tadakuma, T. Funatsu, and S. Ishiwata. 2002. Microscopic analysis of polymerization dynamics with individual actin filaments. *Nat. Cell Biol.* 4:666–673.

Gutsche-Perelroizen, I., J. Lepault, A. Ott, and M. F. Carlier. 1999. Filament assembly from profilin-actin. *J. Biol. Chem.* 274:6234–6243.

Heiss, S., and J. Cooper. 1991. Regulation of CapZ, and actin capping protein of chicken muscle, by anionic phospholipids. *Biochemistry.* 30:8753–8758.

Huxley, H. 1963. Electron microscopic studies on the structure of natural and synthetic protein filaments from striated muscle. *J. Mol. Biol.* 3:281–308.

Isenberg, G., U. Aebi, and T. D. Pollard. 1980. An actin-binding protein from Acanthamoeba regulates actin filament polymerization and interactions. *Nature.* 288:455–459.

Janmey, P., and T. Stossel. 1987. Modulation of gelsolin function by phosphatidylinositol 4,5-bis-phosphate. *Nature.* 325:362–364.

Kang, F., D. Purich, and F. Southwick. 1999. Profilin promotes barbed-end actin filaments assembly without lowering the critical concentration. *J. Biol. Chem.* 274:36963–36972.

Kinosian, H. J., L. A. Selden, J. E. Estes, and L. C. Gershman. 1993. Nucleotide binding to actin. Cation dependence of nucleotide dissociation and exchange rates. *J. Biol. Chem.* 268:8683–8691.

Kirschner, M. W. 1980. Implications of treadmilling for the stability and polarity of actin and tubulin polymers in vivo. *J. Cell Biol.* 86:330–334.

Lassing, I., and U. Lindberg. 1985. Specific interaction between phosphatidyl-inositol 4,5-bisphosphate and profilactin. *Nature.* 314:472–474.

Machesky, L. M., R. D. Mullins, H. N. Higgs, D. A. Kaiser, L. Blanchoin, R. C. May, M. E. Hall, and T. D. Pollard. 1999. Scar, a WASp-related protein, activates nucleation of actin filaments by the Arp2/3 complex. *Proc. Natl. Acad. Sci. USA.* 96:3739–3744.

Maciver, S., H. Zot, and T. D. Pollard. 1991. Characterization of actin filament severing by actophorin from *Acanthamoeba castellanii*. *J. Cell Biol.* 115:1621–1630.

Melki, R., S. Fievez, and M. F. Carlier. 1996. Continuous monitoring of Pi release following nucleotide hydrolysis in actin or tubulin assembly using 2-amino-6-mercapto-7-methylpurine ribonucleoside and purine-nucleoside phosphorylase as an enzyme-linked assay. *Biochemistry.* 35:12038–12045.

Mogilner, A., and L. Edelstein-Keshet. 2002. Regulation of actin dynamics in rapidly moving cells: a quantitative analysis. *Biophys. J.* 83:1237–1258.

Morgan, T., R. Lockerbie, L. Minamide, M. Browning, and J. Bamburg. 1993. Isolation and characterization of a regulated form of actin depolymerizing factor. *J. Cell Biol.* 122:623–633.

Moriyama, K., and I. Yahara. 1999. Two activities of cofilin, severing and accelerating directional depolymerization of actin filaments, are affected differentially by mutations around the actin-binding helix. *EMBO J.* 18:6752–6761.

Mullins, R., J. Heuser, and T. D. Pollard. 1998. The interaction of Arp2/3 complex with actin: nucleation, high affinity pointed end capping, and formation of branching networks of filaments. *Proc. Natl. Acad. Sci. USA.* 95:6181–6186.

Neidl, C., and J. Engel. 1979. Exchange of ADP, ATP and 1: N6-ethenoadenosine 5′-triphosphate at G-actin. Equilibrium and kinetics. *Eur. J. Biochem.* 101:163–169.

Oosawa, F., and S. Asakura. 1962. A theory of linear and helical aggregations of macromolecules. *J. Mol. Biol.* 4:10–21.

Otterbein, L., P. Graceffa, and R. Dominguez. 2001. The crystal structure of uncomplexed actin in the ADP state. *Science.* 293:708–711.

Pantaloni, D., M. F. Carlier, M. Coue, A. A. Lal, S. L. Brenner, and E. D. Korn. 1984. The critical concentration of actin in the presence of ATP increases with the number and concentration of filaments and approaches the critical concentration of actin. ADP. *J. Biol. Chem.* 259:6274–6283.

Pantaloni, D., and M. F. Carlier. 1993. How profilin promotes actin filament assembly in the presence of thymosin β4. *Cell.* 75:1007–1014.

Perelroizen, I., D. Didry, H. Christensen, N. H. Chua, and M. F. Carlier. 1996. Role of nucleotide exchange and hydrolysis in the function of profilin in actin assembly. *J. Biol. Chem.* 271:12302–12309.

Pieper, U., and A. Wegner. 1996. The end of a polymerizing actin filament contains numerous ATP-subunit segments that are disconnected by ADP-subunits resulting from ATP hydrolysis. *Biochemistry.* 35: 4396–4402.

Pollard, T. D. 1986. Rate constants for the reactions of ATP-and ADP-actin with the ends of actin filaments. *J. Cell Biol.* 103:2747–2754.

Pollard, T. D., L. Blanchoin, and R. D. Mullins. 2000. Molecular mechanisms controlling actin filament dynamics in nonmuscle cells. *Annu. Rev. Biophys. Biomol. Struct.* 29:545–576.

Pollard, T. D., and J. A. Cooper. 1984. Quantitative analysis of the effect of Acanthamoeba profilin on actin filament nucleation and elongation. *Biochemistry.* 23:6631–6641.

Rickard, J., and P. Sheterline. 1986. Cytoplasmic concentrations of inorganic phosphate affect the critical concentration for assembly of actin in the presence of cytochalasin D or ADP. *J. Mol. Biol.* 191:273–280.

Sablin, E. P., J. F. Dawson, M. S. VanLoock, J. A. Spudich, E. H. Egelman, and R. J. Fletterick. 2002. How does ATP hydrolysis control actin's associations? *Proc. Natl. Acad. Sci. USA.* 99:10945–10947.

Safer, D., R. Golla, and V. Nachmias. 1990. Isolation of a 5-kilodalton actin-sequestering peptide from human blood platelets. *Proc. Natl. Acad. Sci. USA.* 87:2536–2540.

Schafer, D. A., P. B. Jennings, and J. A. Cooper. 1996. Dynamics of capping protein and actin assembly in vitro: uncapping barbed ends by polyphosphoinositides. *J. Cell Biol.* 135:169–179.

Selden, L., H. Kinosian, J. Estes, and L. Gershman. 1999. Impact of profilin on actin-bound nucleotide exchange and actin polymerization dynamics. *Biochemistry*. 38:2769–2778.

Sept, D., J. Xu, T. D. Pollard, and J. A. McCammon. 1999. Annealing accounts for the length of actin filaments formed by spontaneous polymerization. *Biophys. J*. 77:2911–2919.

Stossel, T. P. 1993. On the crawling of animal cells. *Science*. 260:1086–1094.

Teubner, A., and A. Wegner. 1998. Kinetic evidence for a readily exchangeable nucleotide at the terminal subunit of the barbed ends of actin filaments. *Biochemistry*. 37:7532–7538.

Theriot, J., and T. Mitchison. 1991. Actin microfilament dynamics in locomoting cells. *Nature*. 352:126–131.

Walsh, T. P., A. Weber, J. Higgins, E. Bonder, and M. S. Mooseker. 1984. Effect of villin on the kinetics of actin polymerization. *Biochemistry*. 23:2613–2621.

Wanger, W., and A. Wegner. 1987. Binding of phosphate ions to actin. *Biochim. Biophys. Acta*. 914:105–113.

Wegner, A. 1976. Head to tail polymerization of actin. *J. Mol. Biol*. 108:139–150.

Woodrum, D. T., S. A. Rich, and T. D. Pollard. 1975. Evidence for biased bidirectional polymerization of actin filaments using heavy meromyosin prepared by an improved method. *J. Cell Biol*. 67:231–237.

Yarar, D., W. To, A. Abo, and M. D. Welch. 1999. The Wiskott-Aldrich syndrome protein directs actin-based motility by stimulating actin nucleation with the Arp2/3 complex. *Curr. Biol*. 9:555–558.

Yarmola, E. G., S. Parikh, and M. R. Bubb. 2001. Formation and implications of a ternary complex of profilin, thymosin beta 4, and actin. *J. Biol. Chem*. 276:45555–45563.

Yin, H., J. Hartwig, K. Marayama, and T. Stossel. 1981. Ca^{2+} control of actin filament length. Effect of macrophage gelsolin on actin polymerization. *J. Biol. Chem*. 256:9693–9697.

Yin, H., and T. Stossel. 1979. Control of cytoplasmic actin gel-sol transformation by gelsolin, calcium-dependent regulatory protein. *Nature*. 281:583–586.